Plastic Scintillators For The T2K Fine-Grained Detector

by

Martyn Bryant

MSci., Royal Holloway, University of London, 2005

A THESIS SUBMITTED IN PARTIAL FULFILMENT OF
THE REQUIREMENTS FOR THE DEGREE OF

Master of Science

in

The Faculty of Graduate Studies

(Physics)

The University Of British Columbia

August 30, 2007

Abstract

The T2K Neutrino Oscillation experiment consists of a ν_μ beam produced at JPARC and two detectors: one placed280m downstream, the near detector, and Super-K, which sits 295km downstream. The goal of the experiment is measure the θ_{13} mixing angle and the phase δ found in the MNSP neutrino mixing matrix by measuring the disappearance of ν_μ from the original neutrino beam and appearance of ν_e in the beam as it reaches Super-K. The near detector contains a FGD (Fine Grained Detector) which is designed to provide target mass for the ν_μ and then track the particles which come out once the ν_μ has reacted. The FGD consist mainly of nominally sized 1 cm $\times$ 1 cm $\times$ 200 cm plastic scintillator bars, which are read out by wavelength-shifting optical fibers (which are in turn read out by MPPC photosensors) threaded through each bar. The bars are glued into a series of XY layers.

In November 2006 we successfully extruded 11900 Scintillator Bars at CELCO Plastics in Surrey, BC. On site QA found only 2.5 % of the bars to fall outside of bar specifications. During the November bar production run we scanned 4-10 of each 100 bars within a day of them coming off the production line. We found a variation in the light yields of the bars to be 5 %. We set up an aging test for the bars. Three separate measurements were consistent with a 2% per year aging rate. In December 2006 we put our new bars in the M11 beam line at TRIUMF. The light yield of the bars was measured using MIPS. With the beam hitting the far end of the bar and no reflector on the end of the bar the light yield and was found to be adequate for the FGD. I predicted, using a simulation, the difference in light collected by 2 sizes of MPPC, one 1 mm sq and one 1.3 mm sq with a gap of 0.4 mm between fiber and photosensor to be 25 %. This was in good agreement with Kyoto groups direct measurement.

Table of Contents

List of Tables

List of Figures

Chapter 1

Introduction to Neutrino Physics

1.1 The Neutrino

The neutrino is a member of the lepton family of particles. It is chargeless and so doesnt interact electromagnetically; it is colourless and so doesnt interact via the strong force. The neutrino interacts only via the weak nuclear force and gravity. Neutrinos are extremely abundant and originate from wherever there may be nuclear reactions. In fact, of the ones originating from the sun 5×10^{16} [1] pass through our body every second. Luckily they interact with matter very rarely and so we dont notice them. For this same reason however they are also very difficult to detect and so require very large detector volumes or artificial neutrino beams.

There are 3 different types or flavours or neutrinos: the electron neutrino ν_e, the muon neutrino ν_μ and the tau type neutrino ν_τ. Each get their name from their partner leptons: the electron e, muon μ and tau τ. Whenever a certain type of neutrino is created or destroyed in a charged current interaction it's partner lepton is always present to make up the numbers, hence the naming. Perhaps the most interesting property of a neutrino is that as it propagates it can change between types. Thus a ν_e starting out may change to a ν_μ or ν_τ along its way. This changing of types is known as a neutrino oscillation.

1.2 Neutrino Oscillation formalism

To understand neutrino oscillations some quantum mechanics is needed. As particles propagate they pick up a phase in their quantum mechanical wave function of,

$$\phi(\vec{x}, t) = e^{-i(\vec{p}\cdot\vec{x} - Et)/\hbar}. \tag{1.1}$$

Here $\vec{x}$ is the displacement of the particle, $\vec{p}$ is the momentum, t is the

time and E is given by the relativistic relation,

$$E = \sqrt{|\overrightarrow{p}|^2c^2 + m^2c^4}. \tag{1.2}$$

Here c is the speed of light and m is the mass of the particle. Working backwards through these two equations, a particle with a fixed momentum will have an energy depending on its mass and so will pick up a phase depending on its mass too. A mass eigenstate is one which obeys equation 1.2. A mass eigenstate can propagate happily without any change in its properties, however a linear combination of different mass eigenstates will have interference effects as the phases progress at different rates. Let's follow through this argument for neutrinos. Each neutrino flavour eigenstate $|\nu_\alpha\rangle$ can be expressed in terms of a linear combination of 3 mass eigenstates $|\nu_1\rangle$, $|\nu_2\rangle$ and $|\nu_3\rangle$ by,

$$|\nu_\alpha\rangle = \sum_{j=1}^{3} U_{\alpha j}|\nu_j\rangle, \tag{1.3}$$

where a_j gives the contribution of each mass eigenstate to the neutrino eigenstate.

Alternatively this can be written as

$$\begin{pmatrix} |\nu_e\rangle \\ |\nu_\mu\rangle \\ |\nu_\tau\rangle \end{pmatrix} = \begin{pmatrix} U_{e_1} & U_{e_2} & U_{e_3} \\ U_{\mu_1} & U_{\mu_2} & U_{\mu_3} \\ U_{\tau_1} & U_{\tau_2} & U_{\tau_3} \end{pmatrix} \begin{pmatrix} |\nu_1\rangle \\ |\nu_2\rangle \\ |\nu_3\rangle \end{pmatrix} \tag{1.4}$$

This is known as the Maki-Nakagawa-Sakata or MNS matrix and is believed to be a unitary matrix.

Since U is unitary it can be parameterized and then factorized into 3 orthogonal matrices, since U is unitary,

$$\begin{pmatrix} \cos\theta_{12} & \sin\theta_{12} & 0 \\ -\sin\theta_{12} & \cos\theta_{12} & 0 \\ 0 & 0 & 1 \end{pmatrix} \begin{pmatrix} \cos\theta_{13} & 0 & \sin\theta_{13}e^{i\delta} \\ 0 & 1 & 0 \\ -\sin\theta_{13}e^{-i\delta} & 0 & \cos\theta_{13} \end{pmatrix} \begin{pmatrix} 1 & 0 & 0 \\ 0 & \cos\theta_{23} & \sin\theta_{23} \\ 0 & -\sin\theta_{23} & \cos\theta_{23} \end{pmatrix} \tag{1.5}$$

The parameters θ_{12}, θ_{13}, θ_{23} and δ are the neutrino oscillation parameters which are commonly referred to in the literature. An additional matrix could be added whose parameters are related to another phenomenon being investigated, that of neutrinoless double beta decay. This effect has nothing to do with the oscillation problem and so I have omitted it. The next

two equations show the transformations needed to get from the mass eigenstates to the neutrino eigenstates (Equation 1.6) and back from the neutrino eigenstates to the mass eigenstates (Equation 1.7).

$$|\nu_\alpha\rangle = \sum_j U_{\alpha j}|\nu_j\rangle \tag{1.6}$$

$$|\nu_j\rangle = \sum_\alpha U^*_{\alpha j}|\nu_\alpha\rangle \tag{1.7}$$

Here $U_{\alpha j}$ are the elements of the MNS neutrino mixing matrix. The mass eigenstates propagate in accordance with the time-dependant Schroedinger equation,

$$i\hbar\frac{\partial|\nu_j(t)\rangle}{\partial t} = E_j|\nu_j(t)\rangle. \tag{1.8}$$

the solution of which is,

$$|\nu_j(t)\rangle = e^{-iE_jt/\hbar}|\nu_j\rangle \tag{1.9}$$

We can describe a neutrino's flavour state, at a later time t, in term of it initial state. As the flavour states do not obey equation 1.9 we need to transform the initial state $|\nu_\alpha\rangle$ to a mass eigenstate, project this forward in time using equation 1.9, then transform it back to a neutrino eigenstate $|\nu_\beta\rangle$,

$$|\nu_\beta(t)\rangle = \sum_{j,\beta} U_{\beta j}e^{-iE_jt/\hbar}U^*_{\alpha j}|\nu_\alpha\rangle \tag{1.10}$$

The probability that an initial state $|\nu_\alpha\rangle$ will change to a final state $|\nu_\beta\rangle$ is as follows,

$$\begin{aligned} P(\nu_\alpha \longrightarrow \nu_\beta) &= |\langle\nu_\alpha|\nu_\beta(t)\rangle|^2 && (1.11)\\ &= |\sum_j U_{\beta j}e^{-iE_jt/\hbar}U^*_{\alpha j}|^2 && (1.12)\\ &= \sum_{j,k} U^*_{\beta k}U_{\alpha k}U_{\beta j}U^*_{\alpha j}e^{-i(E_j-E_k)t/\hbar} && (1.13)\end{aligned}$$

Neutrinos are ultra relativistic with $E, pc \gg mc^2$ and $E \approx pc$ Therefore we can do an expansion of the relativistic energy relation in order to simplify Equation 1.13

$$\begin{aligned} E &= \sqrt{p^2c^2 + m^2c^4} \\ &= pc\sqrt{1 + \frac{m^2c^2}{p^2}} \\ &\approx pc\left(1 + \frac{m^2c^2}{2p^2}\right) \\ &\approx E + \frac{m^2c^4}{2E} \end{aligned}$$

Its therefore follows that

$$E_j - E_k \approx \frac{\triangle m_{jk}^2 c^4}{2E} \tag{1.14}$$

where $\triangle m_{jk}^2 = m_j^2 - m_k^2$. We can also assume that neutrinos essentially travel at the speed of light and so the distance they travel L in a time t is simply $L = tc$. Making these substitutions into Equation 1.13 gives,

$$P(\nu_\alpha \longrightarrow \nu_\beta) = \sum_{j,k} U_{\beta k}^* U_{\alpha k} U_{\beta j} U_{\alpha j}^* e^{-i\triangle m_{jk}^2 c^3 L/2\hbar E} \tag{1.15}$$

Let's unravel this expression assuming only 2 neutrinos existed in nature. The mixing matrix for 2 neutrinos would be of the form,

$$U = \begin{pmatrix} \cos\theta & \sin\theta \\ -\sin\theta & \cos\theta \end{pmatrix}, \tag{1.16}$$

and so the probability for one neutrino to change to another would be,

$$P(\nu_\alpha \longrightarrow \nu_\beta) = \sin^2 2\theta \sin^2(\triangle m_{jk}^2 c^3 L/2\hbar E). \tag{1.17}$$

Conventionally, for ease of use, Equation 1.17 is expressed as,

$$P(\nu_\alpha \longrightarrow \nu_\beta) = \sin^2 2\theta \sin^2\left(1.267 \frac{\triangle m_{jk}^2}{eV^2} \frac{L}{km} \frac{GeV}{E}\right) \tag{1.18}$$

Therefore if we measure the change in the flavour of a number of neutrinos with an energy E and over a distance L we can get at the parameter $\triangle m_{jk}^2$. Therefore we can't get at the absolute masses of the mass eigenstate, we can only get at the difference between the square of the masses. This is the same case if there are 3 neutrinos. Oscillation experiments will only give access to the difference of the squares of the masses of the mass eigenstates. The current experimental values for these differences are $\triangle m_{12}^2 = 8.0^{+0.6}_{-0.4} \times 10^{-5} eV^2$ [2] and $\triangle m_{23}^2 = 2.4^{+0.6}_{-0.5} \times 10^{-3} eV^2$ [3].

1.3 Neutrino Oscillation Experiments

Talk of neutrino oscillations first arose when looking at the number of neutrinos that come from the sun. It is possible to make very accurate predictions of the nuclear reactions that are occurring in the sun. From this is possible to predict the number of neutrinos that should be coming from the sun. Work in the 1960s showed, using a large chlorine based detector, that the number of neutrinos reaching us was less that expected [4]. Conclusive evidence came somewhat later however. In 2001 data from the Sudbury Neutrino Observatory, or SNO, found that the number of neutrinos reaching us was actually 1/3 of the ones which set out from the sun [5]. The answer to this was that the neutrinos predicted from the solar neutrino model, more specifically electron type neutrinos, change to muon and tau type neutrinos on their way to us.

Further observations of neutrino oscillations came from looking at atmospheric neutrinos and reactor neutrinos. Atmospheric neutrinos come from the reaction when cosmic rays, particularly protons, hit nuclei in the upper atmosphere. The result is a decay chain which results in predictable numbers of neutrinos, specifically 2 muon type neutrinos to every one electron type neutrino. Cosmic rays arrive at the earths atmosphere isotropically and produce these same ratios of muon to electron type neutrinos in all directions. This means that if we look upwards and downwards from the super-K detector (A 50 kton tank of water surrounded by PMTs located 1km undergroud in Kamioka, Japan. The water is the target for the neutrinos and is the detecting medium for the by-products. Cherenkov light produced from the by-products is detected by the PMTs) the ratio in the fluxes of muon type to electron type neutrinos should be the same. This is not the case however: Assuming these opposite direction are not tangential to the surface of the earth the neutrinos reaching the detector in one direction will have traveled further than the ones coming from the opposite direction and so both will have oscillated by a different amount and so the ratio of fluxes will be different. This has been observed by Super-K [7]

Nuclear reactors also spit out lots of neutrinos at a calculable rate. The KamLAND experiment found a discrepancy [6] between the predicted rate and the observed rate and this was attributed to neutrino oscillations.

1.4 Artificial Beam Experiments

To study neutrino oscillations in a more controlled way it is possible to create a neutrino beam through the decay of pions which are readily producible in particle accelerators. In 1999, the K2K experiment shot a beam of muon type neutrinos from the KEK accelerator in Tsukuba, on the east coast of Japan, to the SuperK detector in Kamioka, 250 km away on the west coast of Japan. The production of muon types neutrinos is as follows:

1. Protons are accelerated in the KEK beam
2. The protons are then directed to strike an aluminium target where many particles such as pions and kenos are produced.
3. Focusing horns producing torroidal magnetic fields then focus the π^+ and K^+ particles into the 200-m long decay pipe where they ultimately decay predominantly into ν_μ's

Front detectors near the beam source were used to measure precisely the flux of ν_μs as well as a low degree of contamination by other types of neutrino. By comparing the front detector measurements to what Super-K observed, it was therefore possible to look for effects of neutrino oscillation and, more specifically, ν_μ disappearance. K2K observed a deficit of ν_μ's compared to the number predicted by the near detectors, providing evidence for neutrino oscillation at 4.3 σ [8].

A second important long baseline neutrino experiment was the MINOS experiment. The MINOS experiment works essentially in the same way as the K2K experiment but has a 730km baseline rather than a 250km baseline. MINOS also looks for a ν_μ disappearance signal and from that data is able to calculate two important parameters to be $\triangle m^2_{23} = 3.05^{+0.60}_{-0.55} \times 10^{-3} eV^2$ and $\sin^2 2\theta_{23} = 0.88^{+0.12}_{-0.15}$ [9]. These results agree with K2Ks finding, but perhaps more importantly the MINOS statistics are higher. There are however no experiments up to now which have made measurements of the MNS mixing matrix parameters θ_{13} and δ. This is mainly due to the low statistics in the KEK and MINOS experiments. The next generation of long baseline neutrino experiments aims to produce a neutrino beam which is 100 times more intense than has ever been made before, and this opens the door to exploring these unknown parameters.

1.5 Physics goals of the T2K experiment

As mentioned before the K2K and MINOS experiments produced relatively low numbers of muon type neutrinos compared to what T2K aims to produce. When a ν_μ is fired it can either oscillate to become a ν_e or ν_τ or it could simply remain as ν_μ having either not oscillated at all or oscillated back to it original flavour. The Super Kamiokande detector in Japan only has the capabilities to see ν_μ and ν_e type neutrinos due to the energy of the neutrino beam. Seeing a drop in the number of ν_μ that would arrive if there were no neutrino oscillations and ν_e consistent with background, it was assumed that the ν_μ oscillated to become ν_τ. From this is was easy to conclude that ν_μ oscillate to become ν_τ, and the mixing angle and mass square differences were estimated. T2K will produce a much higher flux of neutrinos, 50-100 times that of K2K or MINOS, and so it hoped that some ν_e neutrinos will start to appear at Super-Kamiokande significantly above background levels of ν_e from the beam. Then we can get access to the two unknown matrix parameters θ_{13} and δ. From the neutrino mixing matrix it can be shown, after a number of simplifications, that the probability of oscillating from a ν_μ to a ν_e is,

$$P(\nu_\mu \rightarrow \nu_e) = \sin^2(2\theta_{13}) \sin^2(\theta_{23}) \approx \frac{1}{2} \sin^2(2\theta_{13}. \tag{1.19}$$

T2K hopes to observe a ν_e signal which is statistically significant above beam and other backgrounds. From this it is hoped that the upper limit on θ_{13} will be improved by a factor of 20 or a non-zero value will be measured. T2K also hopes to measure the probability of ν_μ oscillating to become ν_x. This should improve the precision of the measurement of $\triangle m^2_{23}$ and $\sin^2 2\theta_{23}$ by a factor of 10. A second phase to the T2K experiment is also in the pipeline. By shooting a beam of $\bar{\nu}_\mu$, and doing the same analysis as proposed for ν_μ, evidence for CP violation can be looked for which will give bounds on the δ parameter.

So in summary the main physics goals of the T2K experiment are,

- A precision measurement of the neutrino oscillation parameters, ($\sin^2 2\theta_{23}$, $\triangle m^2_{23}$) by $\nu_\mu \rightarrow \nu_x$ disappearance.
- The determination of $\sin^2 2\theta_{13}$ by the measurement of the $\nu_\mu \rightarrow \nu_e$ appearance signal.

1.6 T2K

The T2K experiment will fire a man made beam of muon neutrinos produced at the JPARC facility in Tokai, which lies of the east coast of Japan, to Super-Kamiokande 295 km west of Tokai (See Figure 1.1). The neutrino beam will be the most intense beam ever created, 50 times the intensity of the neutrino beam from the K2K experiment.

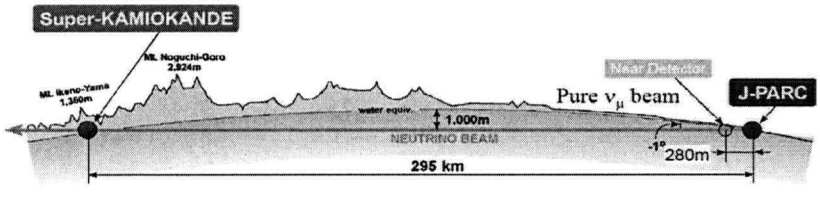

Figure 1.1: T2K Sketch

As the muon type neutrinos fly across Japan they will oscillate into other flavours of neutrinos, the extent of which can be used to calculate neutrino mixing parameters. A detector (called the ND280) is placed at 280m from the start of the neutrino beam to measure the spectra and fluxes of the neutrinos before they oscillate. The Super-Kamiokande will then measure the spectra and fluxes of the neutrinos after they have been oscillating over a 295km distance. The Super-Kamiokande detector is well suited to distinguishing muon type neutrinos from electron type neutrinos due to differences in the Cherenkov light patterns coming from charged-current interactions in its 50 kton water target.

1.7 Beam Production

The muon type neutrino beam is made at the JPARC facility in Tokai (See Figure 1.2). JPARC is an accelerator ring for accelerating protons to 50 GeV. The beam is designed to have an intensity of 3.3×10^{14} protons/pulse and each pulse will pass at a rate of approximately 1 every 3 seconds.

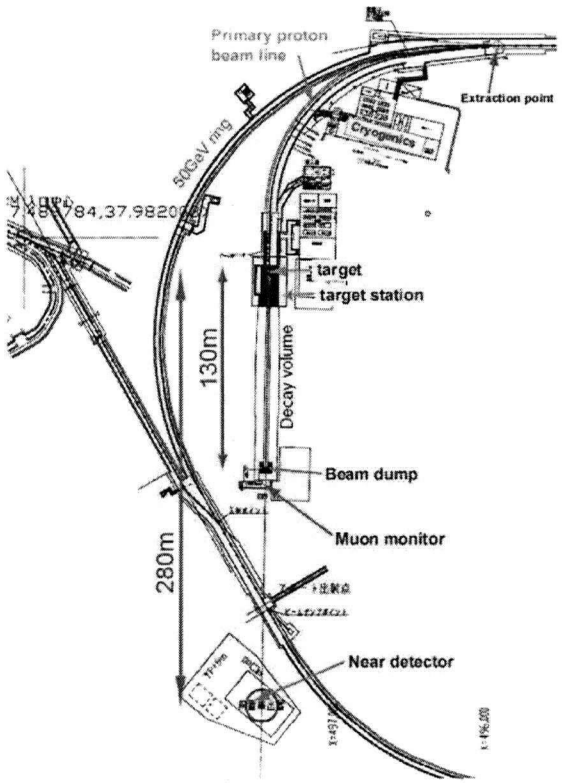

Figure 1.2: Neutrino Production Beams line at JPARC

The protons are steered off the accelerator ring towards a graphite target. The graphite target is cylindrical with a diameter of 3 cm and a length of 90 cm. The beam will hit the end of the cylinder perpendicularly to the end surface of the cylinder. On hitting the graphite target pions (and kaon, which are less useful as they provide a ν_e background when they decay) are produced. Three electro-magnetic horns will be used to focus the charged pions generated in the target to the forward direction. The first horn sits

around the target so that it focuses as many pions as possible from the target. The magnetic field of the horns are synchronized with the arrival of the bunches of protons which arrive at the target. The pions decay to muon and muon type neutrino in a 130 m length decay pipe. The muons are stopped in the muon pit at the end of the decay pipe and so what is left is a beam of muon type neutrinos.

1.8 Off Axis Beam

Due to the nature of the kinematics of a pion decay to muon and muon type neutrino it is possible to have a narrower energy spectrum of neutrinos by having an off-axis detector. The pion beam will be travelling in the same direction as the proton beam. ND280 and Super-K are located 2.5 degrees off this axis. Figure 1.3 shows that if the beam of pions is aimed by the horns to miss the Super Kamiokande detector, by 10km or 20 km as the arrows indicate, the energies of the neutrinos tend to bunch up. Figure 1.4 show 3 neutrino spectra. These spectra are for different off-axis angles as defined above. As the off axis angle increases the flux of the highest energy neutrinos is lowered (high energy ν_μ can produce π_0 in Super-K which may look like ν_e signal) and the energy spectrum narrows. T2K expects to set an off-axis angle so that the neutrino energy is bunched between around 0.5 to 0.9 GeV, the peak oscillation energy being around 0.7 GeV. I short, the off-axis technique allows T2K to increase the flux at the expected peak of the oscillation probability (around 0.7 GeV), while suppressing backgrounds from higher energy neutrinos.

1.9 ND280

1.9.1 Role of the ND280

The ND280 (Near Detector at 280m) is designed to measure the muon type neutrino spectra and fluxes before they have a chance to oscillate and to measure any $\neq_e$ background in the beam . It will do this by measuring the rates of the different possible reactions of the incident neutrinos with the detector. The most common reaction to occur in the detector is known as a CCQE (Charged Current Quasi-Elastic) reaction. At the proton beam energy and off-axis angle we plan to use, 37% of the events are expected to be CCQE. The CCQE reaction is,

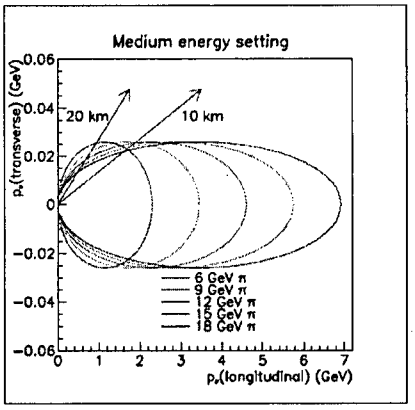

Figure 1.3: Plot showing pions of different energies giving ν_μ of the same energy when viewed of-axis, as indicated by the overlap of the ellipses where they cross the two arrows representing 2 different neutrino directions.

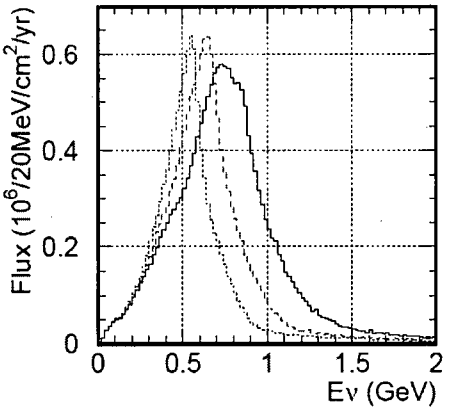

Figure 1.4: Energy spectra from off-axis beams: black-solid line (2 degree), red-dashed line (2.5 degree), and blue-dotted line (3 degree). As the off-axis angle increases, the energy peak narrows and moves lower in energy.

$$\nu_\mu + n \rightarrow \mu^- + p. \tag{1.20}$$

It is called a charged current interaction as the propagator in the reaction is a charged W boson. The incident muon type neutrino hits a neutron in the detector and results in the production of a proton and a muon, both of which will be tracked to get their momenta. From this the energy of the muon type neutrino can be reconstructed. Our detector needs to have the capabilities to measure the momentum of the particles produced from these reactions and for that reason is made up of a few different types of detectors (Time Projection Chambers, Plastic Scintillator Detectors, Electromagnetic Calorimeters etc).

1.9.2 Components of the ND280

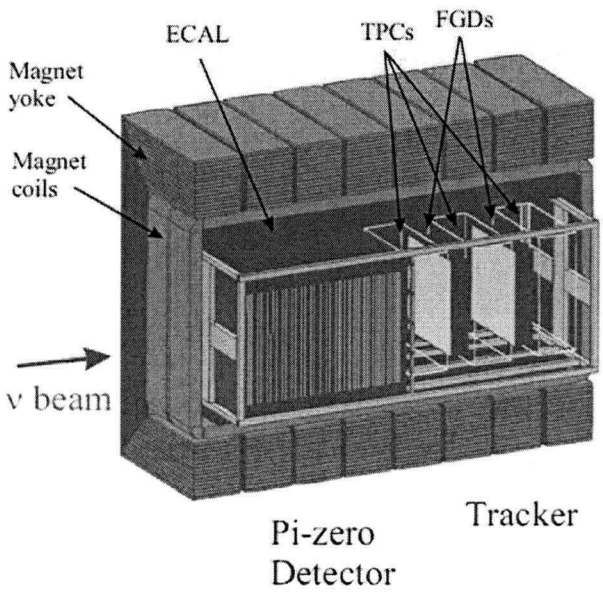

Figure 1.5: The ND280 detector (Near Detector, 280 m from the graphite target)

The ND280 is essentially made up of five parts: A π_0 detector to detect particles from neutral current interactions; a tracker to detect charged particles produced from charged current interactions; a electromagnetic calorime-

ter to detect photons from the detector; an SMRD (Side Muon Range Detector) to detect muons produced at large angles with respect to the beam direction and the 0.2T UA1 Magnet to provide a magnetic field for the tracker.

1. Pi-Zero Detector (P0D): The P0D is designed to measure the rate of neutral current π^0 production and the detector sits at the upstream end of ND280. The P0D is made up of tracking planes which are composed of scintillating bars alternating with lead foil. Inactive layers of passive water in sections of the P0D provide a water target for measuring interactions on oxygen (this too is the case for the FGD).

2. Tracker: Downstream of the P0D is a tracking detector. It is designed to measure the momenta of charged particles produced by CC interactions, in particular pions and muon. The tracker consists of 3 TPCs and 2 FGDs.

    - Time Projection Chambers (TPCs): The TPCs will measure the momenta of muons produced by charged current interactions in the detector. This will provide the most accurate measurement of the neutrino energy spectrum. The curve of the particle track will also determine the sign of charged particles and will enable the identification of muons, pions, and electrons.

    - Fine Grained Detectors (FGDs): The FGDs provide the target mass for neutrino interactions that will be measured by the TPCs. The FGD will also measure the direction and ranges of recoil protons produced by CC interactions. This will give clear identification of whether an event is CCQE or not. The FGD modules consist of layers of finely segmented scintillating tracker bars. There are two FGDs in total. One FGD module will consist entirely of plastic scintillator. The second will consist of part plastic scintillator and part water. The water is present to allow the separate determination of exclusive neutrino cross-sections on carbon and on water for comparison with SuperK.

In total there are 3 TPCs and 2 FGDs. As you move in the direction of the beam the ordering of these tracker components is TPC-FGD-TPC-FGD-TPC.

Surrounding the entire detector is an Electromagnetic Calorimeter or Ecal. The Ecal is a segmented Pb-scintillator detector whose main purpose

is to measure those photons produced in ND280 that are not stopped by the inner detectors and is so critical for the reconstruction of π_0 decays. The whole detector (POD, ECAL and Tracker) is surrounded by the UA1 magnet. This is in place to provide the magnetic field necessary to bend the muon tracks in the TPC so that their momentum can be measured. The UA1 magnet also contains a series of gaps as you move away from the center of the detector. Most of the gaps will contain an instrumented slab of scintillator which will be able to measure the range of muons which, originating in the FGD, travel at a large angle w.r.t the beam direction and consequently never pass through one of the TPCs. As the SMRD is the first detector to be seen by cosmic neutrinos it can be used as a good scintillator counter for calibrations in the inner detector.

1.9.3 Closer look at the FGD

The target mass for the neutrino is polystyrene scintillator. This is polystyrene which has been mixed with PPO and POPOP dopants to make polystyrene's scintillation light visible. Once the neutrino has interacted with the plastic the charged particles created will deposit energy in the scintillator which will be turned into light which we can then read out.

Each FGD is made up of nominally 2m by 1cm by 1cm polystyrene bars to make a complete FGD which is 2m wide by 2m high by 30cm deep. To do this the FGD is made up of 30 layers. The first layer is made up of 200 bars placed vertically next to each other to make a 2m by 2m by 1cm plane. The next plane is identical but the bars are lying in the horizontal direction. These two planes with the bars rotated 90 degrees between them are collectively known as an X-Y layer. To completed the rest of the FGD 14 more X-Y layers are added to make 15 in total.

1.9.4 Getting the Scintillated light out from the interaction point

Too keep scintillated light inside our bars each bar has a white reflective coating (a mixture of polystyrene and $Ti0_2$). Now the light has been restricted to the bar it was produced in we need to get it out of the bar before it is reabsorbed. To do this each bar has a 1.8 mm diameter hole running through it and WLS (wavelength shifting) fiber is strung through it. The role of the WLS fiber is to absorb the scintillated light and then re-emit it at a longer wavelength at which point it will travel down the fiber and then can be read out using a photosensor of some sort.

1.9.5 Photosensor and Electronics

The photosensor being used is a Multi Pixel Photon Collector or MPPC. It is a small, typically 1mm square, silicon device which is made up of a matrix of 400 avalanche photodiodes. Its is extremely well suited to resolve individual photoelectrons, has a large dynamic range (1 to 400 photons (I neglect saturation effects)), works at a low operating voltage (around 70 volts, compared to 1000s of volt for PMTs) and works inside a magnetic field. The MPPCs are attached to the photosensor busboard. Here the signal from the MPPC is split into 2 channels, one of which has a high attenuation, the other a low attenuation. The signals then travel to the AFTER ASIC (a chip specially designed for the T2K experiment). The ASIC shapes the signal and then 20 ns bins are sampled and the charge is stored in a switch capacitor array. This analogue array is then digitized using an ADC at which point it is transferred to a crate masterboard which has all the logic for accepting pulses. The pulse information is then sent optically to the DCC (Data Collection Card) and then can be downloaded onto a pc for offline analysis.

1.9.6 Tracking

As each layer is rotated 90° with respect to the previous layer the FGD has tracking capabilities. If a charged particle hits the first x layer the particular bar it went through can be tagged by measuring the light coming from each fiber and seeing which bar produced a flash of light. Similarly as the charged particle passes through the next layer, a y layer, one of the bars will scintillate and we can tell which bar did so by looking for the light coming from the fibers. The two bars that produced light have an coordinate each; the first bar coming from the x layer gives us the x coordinate and the second bar coming from the y layer gives us the y coordinate. Combine this with the z position of the x-y layer we have an x, y and z coordinate for the charged particle. As the particle moves through each x-y layer a 3D coordinate for the particle can be given and so the trajectory the charged particle took can be seen by connecting up these coordinates.

Protons will tend to stop somewhere inside the FGD so they can be tracked until they run out of energy and stop in a bar. Lighter particles will punch through the FGD at which point they can be tracked using the remaining TPCs and FGDs in the particle's path.

Combining the energy and momentum values given to all the particles that came from the neutrino interaction, the energy and momentum of the

incident neutrino can be estimated.

Chapter 2

Bar Production Method

2.1 Introduction

We produced our scintillator bars at CELCO Plastics Ltd in Surrey, British Columbia. Our goal from the beginning was to produce scintillator bars using our own TRIUMF engineers (Naimat Khan), the extrusion line at CELCO and the expert operators working for CELCO. This Chapter explains how the bars are produced, how we learnt from pre-production runs, the full production run itself and the Quality Assurance tests the bars underwent after they came off the production line.

2.2 Plastic extrusion

Plastic extrusion is the process whereby molten plastic is passed through a die to give the desired cross-sectional shape and size of a essentially infinite (material permitting) length piece of plastic. In our case we want to produce bars which have a square cross-section (approx 1 cm by 1 cm) and are nominally 2m long. To get the 2 m length bars is simple. As the continuous bar comes through the die, it is cooled down and then cut to 2 m lengths. The exact cross sectional specifications is difficult to come by and this is the art of extrusion. To make things even more difficult we wanted to co-extrude our scintillator bars. This means we wanted to extrude bars with the TiO_2 coating as well. To get the reflective coating onto the surface of the bars, as the scintillator passes through the die molten reflective coating can be injected onto the surface of the scintillator. To get the desired thickness of coating and overall cross-sectional size of the bar is all done though trial and error (explained later). The bar also has a hole in it. This is created by having a long needle run through the center of the die. Figure 2.1 shows a cross-section photo a scintillator bar.

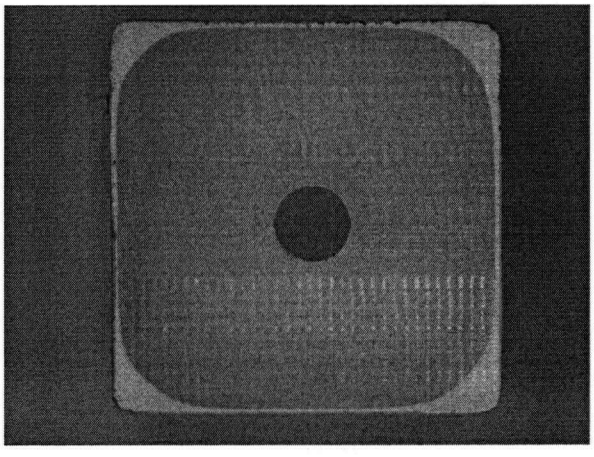

Figure 2.1: Cross-section photo of a pre-production bar. There is a white TiO_2 coating surrounding the bar. There is also a hole in the center of the bar for the Wavelength shifting fiber to go through

2.3 Mixing Materials at TRIUMF

The materials and mixing procedures are identical to those utilized in producing extruded scintillator strips for MINOS and the K2K SciBar detector. The mixing for our production run was done by Doug Mass.

- The polystyrene pellets were weighed in 100 lb. batches and dried for 8 hours at 170F under dry N_2; then mixed under dry N_2 with the premixed PPO/POPOP fluor; then stored in 200 lb. containers under dry N_2 purge. Per 100lb of polystyrene pellets 460 grams of PPO and 13.6 grams of POPOP. The premixed PPO/POPOP fluor was supplied by CURTISS laboratories, inc.

- Each container was bar-code labeled to record date, mixing conditions and mixing crew.

- The TiO_2 coating (15 lbs polystyrene to 5 lbs TiO_2 concentrate) was mixed by hand and similarly dried and stored in bar-code labeled buckets under dry N_2. The TiO_2 was supplied by Clarient - Masterbatches Division (Product: WHC-25311-A. Plastic compound, lot number: am6102)

- The mixed materials were transported to Celco., where they were purged with dry N_2, then fed into hoppers. The mixes were purged

with N_2 to keep out any moisture in the air; this is said to lower the light yield of the scintillator if not removed. Separate hoppers were used for the doped plastic scintillator extrusion and for the TiO_2 co-extrusion.

2.4 Bar Production Method

The bar production process is as follows

1. The plastics, dopants and TiO_2 are mixed and dried at TRIUMF. See section on mixing.
2. At CELCO the scintillator mixes are stored in drums and purged with N_2.
3. When needed, the scintillator mix is loaded into the main hopper and the TiO_2 coating mix is loaded into the side hopper (seen in the back of Figure 2.3)
4. The scintillator mix is melted down and pushed through the die using a screw
5. As the scintillator passed through the die the TiO_2 coating mix is melted down and injected onto the surface of the scintillator
6. through the center of the die runs a long needle. The needed is there to create a hole.
7. The co-extruded bar and coating then passed through a sizer plate which will set the final dimensions of the bar (See Figure 2.2)
8. After the sizer plate the bar passes through a warm water bath where it cools down (See Figure 2.4)
9. The bar then passes through a conveyor belt which pulls the bar through the whole production line (See Figure 2.5)
10. After that the bars are cut to length and then the QA steps takeover.

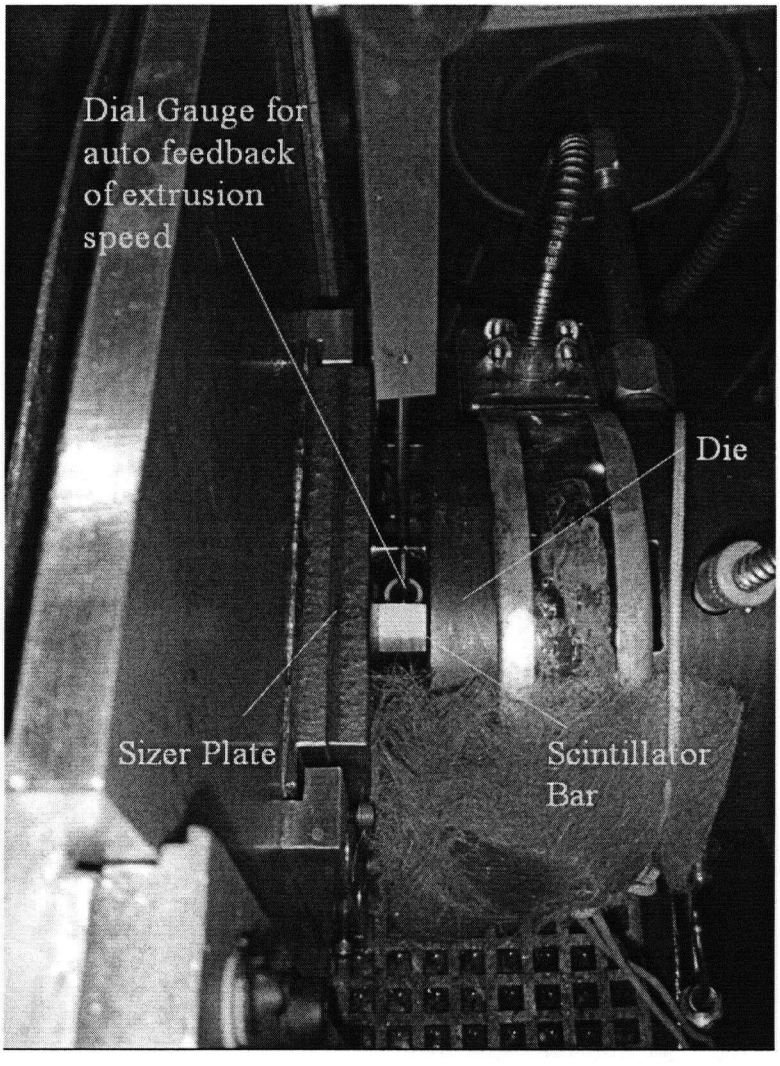

Figure 2.2: Extruded plastic being pushed out of the extruder and through the sizer plate into the water bath. The feedback dial gauge is in place to detect changes in the thickness of the bar once it has been pushed through the die. If the bar gets wider the extruder screw speed will decrease and if the bar gets narrower the extruder screw speed will increase.

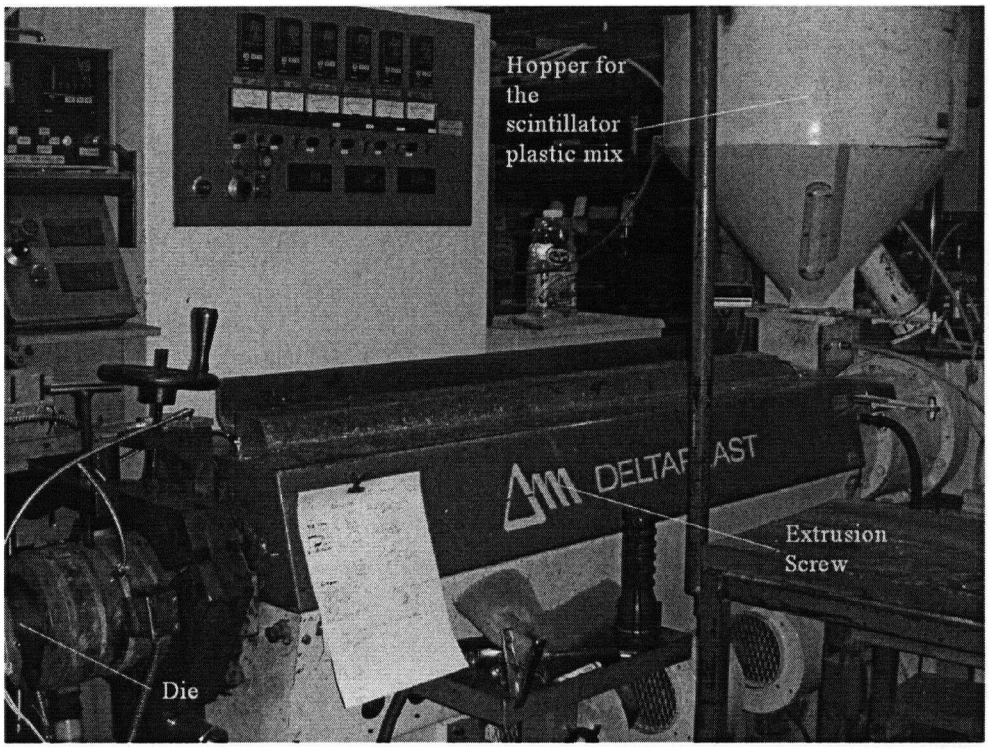

Figure 2.3: Full view of extruder itself

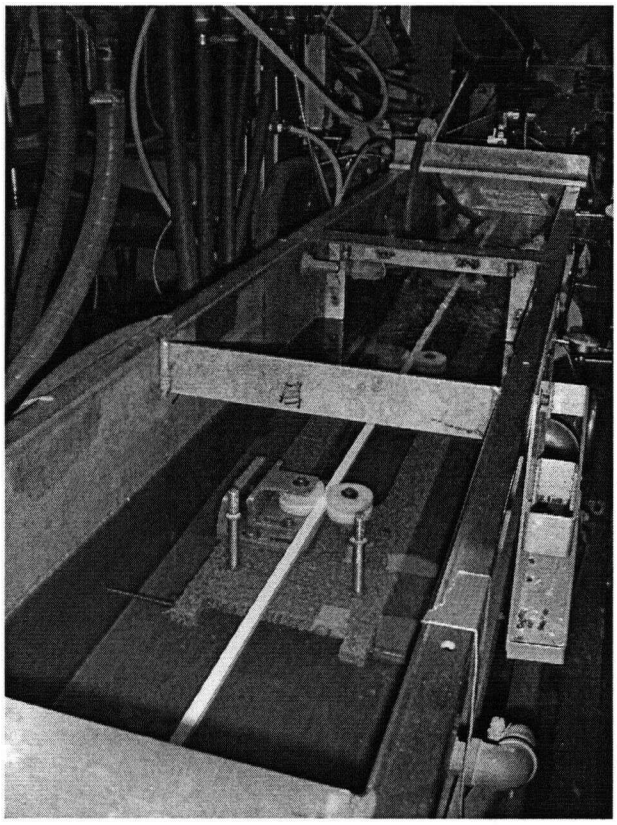

Figure 2.4: water bath to cool the plastic down once it has passed through the sizer plate

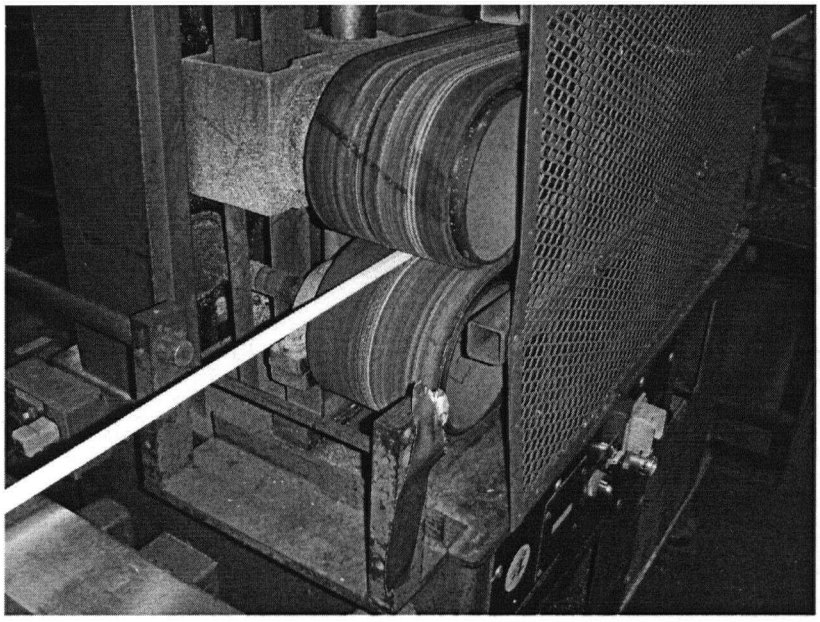

Figure 2.5: Conveyor belt to pull the bar through the production line

2.5 Pre-production runs

Extrusion is an art and not a science. We needed a few iterations before final production so we could perfect our technique. These included; adjusting the shape and size of the die to give us square bars; adjusting the size of the needle to get the correct hole size; adjusting the flow of TiO_2 onto the surface of the scintillator to get the correct amount of coating and many more.

Figure 2.6 is interesting. It shows the cross section of two bars produced on two consecutive days in February 2006. The difference between the two comes from changing the shape of the sizer plate very slightly. As the molten scintillator bar passes through the sizer plate into the water bath it cools down fairly rapidly. This cooling occurs quicker on the surface of the bar and so results in a bar with concave edges. To counter this we changed the square in the sizer plate so that the edges were rounded outwards slightly.

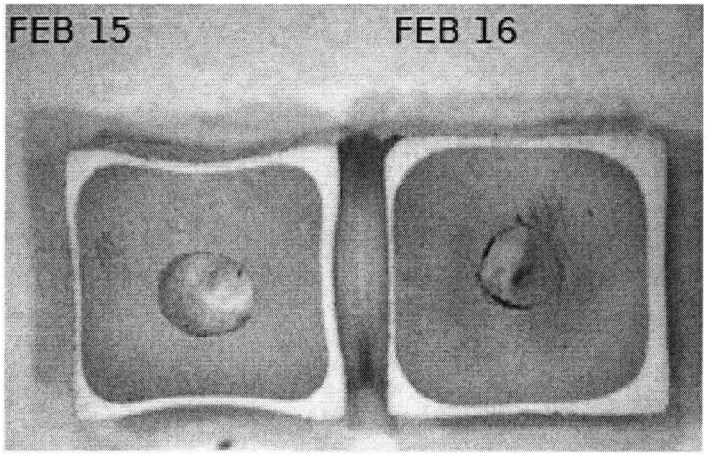

Figure 2.6: Figure showing cross section of a bars produced in a pre-production run. To get from the left bar to the right bar we changed the shape of the sizer plate.

Figure 2.7 shows a cross section of a bar produced in our final pre-production run. Many fine adjustments were made from the run in February but most emphasis was put on decreasing the thickness of the $Ti0_2$ and making sure it was uniformly distributed on all four sides of the bar. The thickness was decreased by decreasing the speed of the co-extrusion screw (the screw which pushes the TiO_2 mix onto the surface of the scintillator). To make the TiO_2 thickness even on each side we chose to inject the TiO_2

from both the left and the right sides instead of just from the left side as we did in previous extrusions. Figure 2.7 shows how we were successful at that. We were then happy to go into the final production run with the current extruder settings.

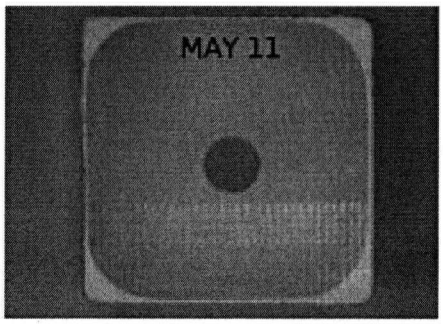

Figure 2.7: Cross-section of a bar produced in May 2006

2.6 Shift Responsibilities

Once in full production we ran for 3 weeks, 24 hours per day. Peter Kitching compiled a shift schedule where 8 hour shifts were allocated to members of the group. The shift responsibilities for each shift worker were as follows.

- Loading material into the hoppers
- doing on-site QA to check dimensions and that the holes through the bars are clear
- keeping a logbook and fixing a barcode label on each bar. The label would enable the bar to be correlated to date/time of production, mixing batch etc.
- packing the bars for shipment to Triumf
- transporting the bars back to Triumf at the end of the shift
- keeping material under dry N_2 purge
- swapping dry N_2 dewars if one runs out

2.7 Bar Quality Assurance

We had a list of specifications we wanted our bars to meet.

- Length (z dimension) = 1843.2±1.0 mm
- Outside x and y dimensions = 9.65 ±0.2 mm
- TiO_2 thickness = 0.250±.05 mm, (co-extruded bar coating)
- Active dimensions = 9.1±0.3 mm
- Hole diameter = 1.8±0.3 mm

During the production run there were various QA steps taken to insure the bars met these specifications.

1. Each bar was labeled with a bar code (bar code and number) just after it was cut by the saw.
2. Burrs were removed from the holes and the edges of the bar using a utility knife.
3. The bar was fed into the x-y direction measuring jig
4. A stainless steel rod was threaded through the bars hole to check for blockages.
5. The bar code was then scanned which automatically got the computer to read out the x-y width values of the bar. This information was stored with a time stamp to go with it.
6. If the bar was out of tolerance (9.65 +/- 0.1 mm) the attention of a CELCO operator was raised to investigate the change.
7. Every 1-2 hours or so a small (approx 5cm) piece of scintillator was cut and polished using successively fine graded sandpaper. The bar was then placed into the holding jig so that a photo of the end of the bar could be taken. Some matlab software was written to analyze the photo taken. It had an edge finding routine which could be used to find the $Ti0_2$ boundaries or hole boundaries and from that their dimensions could be measured. See Figure 2.9 for a photo of a bar with the dimensions drawn on.

8. After every shift the bars produced during the shift were taken back to TRIUMF. 4-8 Bars out of every 100 were scanned on the bar scanner (See Chapter 3) to make sure the light yield was ok. If not there could be a problem with the mixing of the dopants with the polystyrene and it would have needed to have been set straight.

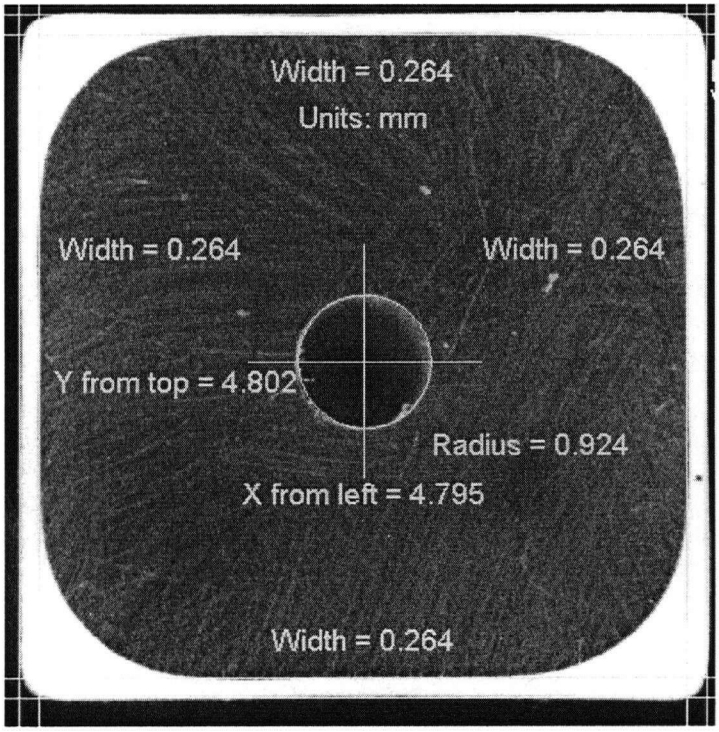

Figure 2.8: Photo taken by the CCD camera based at CELCO. A Matlab edge-finding routine is used to find the edges of the TiO_2, to get the TiO_2 thickness on all 4 sides, and the edge of the center hole, to get the hole diameter.

2.8 Bar Width Results

This section summarizes the results of the dial gauge measurements on the bars as they came off the production run at CELCO Plastics. There were 4 dial gauges in total: 2 to measure the width of the bar in the x direction and

two to measure the width of the bar in the y direction. Figure 2.9 shows one x and y pair of the 2 pairs of dial gauges. Two spring-loaded pins are pushed against the bar and the dial gauge, also spring-loaded and pre-calibrated, also pushed against the bar to get the dimensions. The resolution of the dial gauges is 0.01 mm. Once the scintillator bar is in place the 4 dial gauges are readout using the laptop computer.

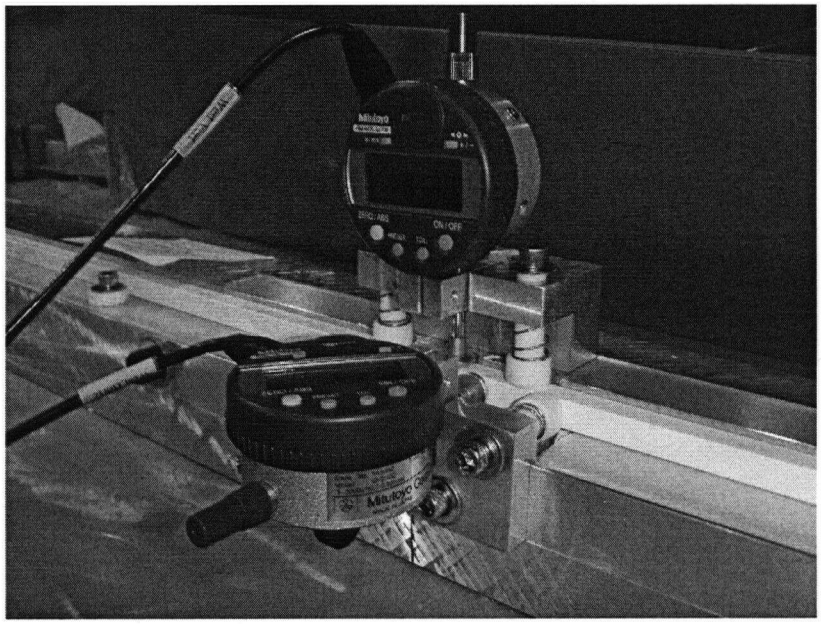

Figure 2.9: Bar width measurement jig

Figure 2.10 shows a trend plot of the width of the bar over the first 9000 bars of the production run. The width of the bars in the y direction stays fairly constant over the run with perhaps a slight peak. The width in the x direction however increases by 0.05 mm from the first bar to the 5000 bar and then back down again. The bars are all within the specified tolerances of 9.60 $\pm$0.2 mm.

Figure 2.11 shows these widths put into histograms. The widths of these bars are all close to 9.6 mm as required but the width in the y direction is slightly less (order of a few hundredths of a mm) than the width in the x direction.

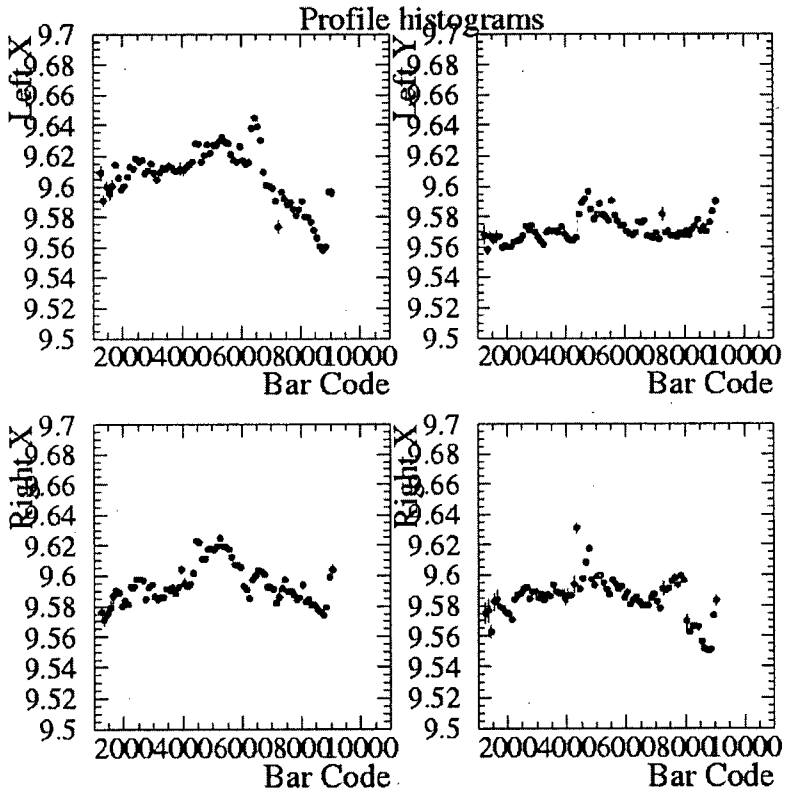

Figure 2.10: Figure showing the width of the bars, as measured by the dial gauges, over the first 9000 bars of the production run

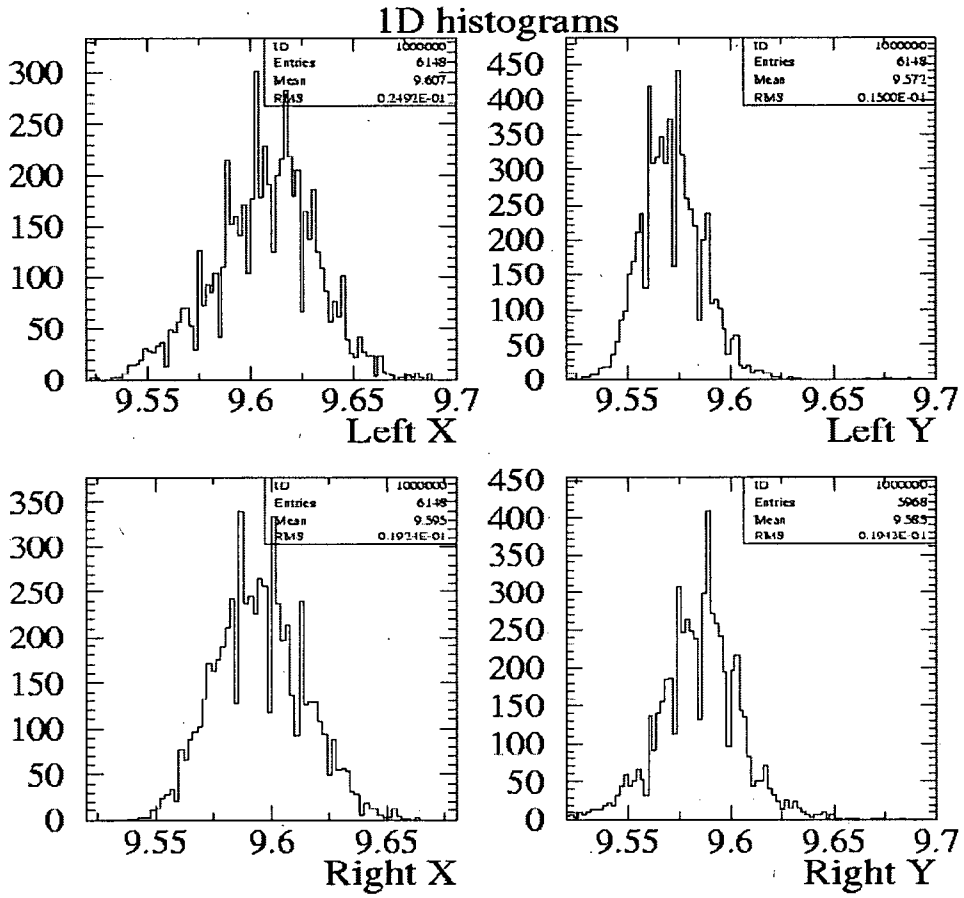

Figure 2.11: Figure showing histograms of the widths as measured by the dial gauges

2.9 Final Count

The first FGD consists of 15 XY-layers, 5760 bars. The second FGD is a water-rich detector consisting of 7 XY-layers (2688 scintillator bars), alternating with six 2.5cm thick layers of water (15 cm total thickness of water). Therefore the total number of bars required = 5760 + 2688 = 8448 (plus spares we think 10000 bars are needed)

In a 3-week production run at the factory of Celco Plastics, starting November 14, 2006, we produced bars 24/7 at the rate of 1bar/every 2 minutes. In the end we chose to continue the production run until all of the material had been used up. This gives us a total number of approximately 11900 bars with reject rate from our QA of just 2.5%.

Chapter 3

Bar Scanner Hardware and Controls

We wanted to make a bar scanner which could run a radioactive source along a bar, which has a WLS fiber running through it, and measure the light output as a function of position. With this data we could;

1. look for dead spots (areas of the bar which scintillate less than the rest of the bar)
2. compare light yields between the bars as they came off the production line
3. measure the attenuation length of the scintillator and fiber

3.1 Photosensor

We decided we would use a photodiode to detect the light coming from the end of the WLS fiber. To minimize noise due to gain fluctuations we didn't have the photodiode hooked up to any bias voltage and so it would be used as a photovoltaic cell. We could detect the current, which would be of the order of pA, by directly connecting the photodiode to a Keithley picoammeter using a piece of coax cable. We used 2 different sized photodiodes from Hamamatsu: The S2386-18K, with a 1.1mm x 1.1mm active area and the S2386-5K, which has a 2.4mm x 2.4mm active area. The 1.1 mm sq device came in the TO-18 packaging which is the same packing as for the Russian SiPM. This meant that we could use our previously fabricated fiber-Russian SiPM couplers to couple the fiber to the photodiode. The photodiode however comes with an air gap and a glass window in front of it. The fiber therefore wouldn't be butted directly up against the phtodiode's active area and some of the light from the fiber would be lost. We purchased the larger device as, even though the noise rate would be higher, it would detect more of the light that spread out from the end of the WLS fiber and missed the 1.1 mm sq device.

The larger photodiode came with a larger packaging so a new fiber-photosensor coupler would need to be made.

3.2 Shielding of the photodiode

In the first setup, a 3 ft long piece of coax (one end connected to a BNC connector, the other end open) was soldered to a photodiode. The BNC end of the coax was plugged into a Keithley Picoammeter. To couple the fiber to the photodiode, a cylindrical plastic coupler was made from black acrylic. A hole in one end was made with a lathe so the photodiode could be snapped into place with a good friction fit. In the other end a 1mm diameter hole was drilled so the fiber could be slotted in and butted up against the center of the photodiodes window. A small amount of epoxy could be applied where the fiber goes into the coupler to keep the fiber in place. See Figure 3.1.

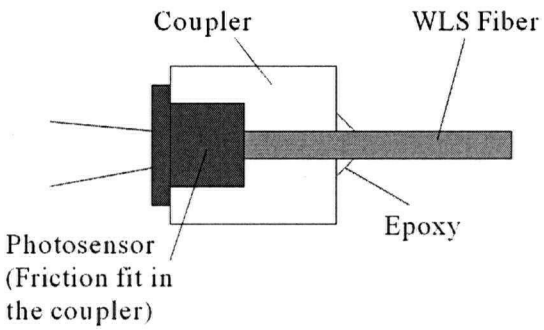

Figure 3.1: Fiber-Photosensor Coupler

A small sample piece of fiber was slotted into the plastic holder, a piece of our scintillator bar was placed over the fiber and everything was put in a cardboard box that could be made light tight.

It was found that if you seal the light tight cardboard box and turn off the room lights there is a lot of noise picked up by the photosensor. I also noted that it seemed to be motion sensitive; the noise would go up if you were moving around and would slowly go down if you were still. When all was stationary the noise rate fell by too slow a rate to make it a practical device to make measurements on.

The first thought was that the coax wire was the cause of this, so I went to the steps of putting a shielding around the entire coax. This was done

by stripping out the central wire of a larger coax wire and then feeding my original coax cable through the larger coax cable. I then had a wire with two layers of braided coax shielding. The outer shielding was connected to the outer casing of the BNC connector to ground it.

This didnt have much effect on the motion sensitivity of the setup so I chose to shield the photosensor itself. I cut a 2 inch long piece of copper pipe (1.5 cm inner diameter and 2-3 mm wall thickness) and placed that over the photosensor and taped the outer coax shielding to it. The noise went from a nA level to hundredths of a pA level after doing this and I was now able to take some first test measurements.

As the process of stripping one coax to feed in another took too much time and we wanted a few of these BNC-coax-photodiode (with shielding) setups, we chose to shield the coax with some braided copper shield which was firmly connected to the outside of the BNC connectors and could be spread apart more easily to get it to go over the copper pipe.

3.2.1 New photodiode-fiber coupler

In the scanners current state, if the fiber was damaged it would be difficult to replace it as it was glued to the photodiode-fiber coupler. We had a new coupler made which also has a good friction fit onto the photodiode, but this time the fiber could be put into place, and two couple screws could be tightened squeezing the plastic coupler onto the fiber so to hold it in place.

3.3 Source

We can now measure how much light comes from the end of a WLS fiber using a photodiode. The next step is to get the scintillator to produce some light. A Sr-90 source was used initially to do feasibility tests e.g. solving the motion sensitivity of the sensor problem. From then on the Ru-106 source was used for the bar scanner. The Ru-106 source produces a higher current than the Sr-90 and also that would free up the Sr-90 source to be used on the aging tests.

In earlier tests we thought we could make a setup which triggered on particles, coming from the source, which passed through the bar. The Sr-90 beta particles, which come out at maximum of 2.284 MeV, don't penetrate through the bar. The Ru-106 decay contains a maximum 3.541 MeV beta particle which would pass through the bar and we could use it for triggering. See Table 3.1 for specific details about the strontium and ruthenium radioactive sources. We found that the Ru-106 beta particles difficult to

trigger on. This was the main reason why we chose to readout the average current from a photodiode for the bar scanner without a trigger rather than counting the number of PEs produced from a particle using a trigger.

3.4 Original Scanner

The original scanner consisted of a frame 20ft long and 4ft high made from I-Beams. A 1ft wide by 4 ft high by 1 cm thick metal train with 2 pinions for wheels sat on a rack which ran the entire length of the frame. A motor (referred to as the X Motor) powered the rotation of one of the pinions so the train could move backwards and forwards along the 20ft of the frame. Mounted to the side of the train, running from top to bottom, was a 4ft screw. A metal plate was attached to the screw via a 2 inch long nut. This plate wouldnt rotate around the screw as it was held by a second metal rod which sat to the side of the screw. Therefore, when the screw is rotated, the nut, and therefore the metal plate, moves up and down. A motor (referred to as the Y Motor) was connected to the top end of the screw and so rotating the screw one way would cause the plate to move up and vice versa. The motors were connected to controllers which would supply power to the motors to move the metal plate.

So the train didn't run off the end of the rack two limit switches were added such that when the train got to the end of the track they were pressed and the power would be cut off to the X Motor. Similarly if the nut got

Table 3.1: Source Properties. The typical current is when the source is placed on the bar 20cm from the photodiode.

Source	Half-life	Radiation	Average Energy	Maximum Energy	Activity (11th Sept 2006)	Typical Current
Sr-90	29.1 years	β	0.196 MeV	0.546 MeV		
$\Downarrow$						
Y-90 (daughter)	spontaneous	β	0.935 MeV	2.284 MeV	70 μCi	2.65 pA
Ru-106	1.02 years	β	1.508 MeV	3.541 MeV	101.5 μCi	3.85 pA

to the top or bottom of the screw it would jam the screw and stop it from rotating. Limit switches were mounted on the metal plate so that if it got too high or low the switches would be pressed and the power would be cut to the Y Motor.

3.5 Scanner Table

Figure 3.2 is a schematic diagram of the bar scanner. Our first step towards this setup was to make a horizontal surface for our scintillator bars to sit on. We used an L beam for this which was clamped to the uprights at each end of the original frame. We checked that it was level using a spirit level. One problem we had was that due to the weight of the L Beam and with it only being supported at either end it would sag slightly in the middle. To get around this we put a table under the middle of the bar and added wooden shims to prop up the bar to keep it level.

We found that if you slid a bar across the metal beam some of the metal would rub off on the bar and discolour it. To protect the bars as they slid across the surface of the table a layer of masking tape was laid down.

Two guidance rails (surrounded in masking tape) were also added. One was clamped onto the back of the L beam so the bar would not fall off the back. The second laid flat on the nearside of the bar and was simply pressed up against the bar, it's own weight stopping it from being pushed back if a bar was not straight, etc. Pressing the flat guidance rail against the scintillator bar insured that each bar sat in the same position relative to the source.

3.6 Source Holder

I noted in earlier tests that if you were 1 or 2 mm off in the positioning of the source from the center of the bar, that would give 30-40 % less light that if you put if perfectly in the center of the bar. This is due to the dimensions of the source, the dimensions of the window in front of the source, and the dimensions of the bar itself. Simply, when you move the source to one side fewer of the beta particles from the source get into the bar. It was therefore critical in designing the source holder for the scanner that the source would be reproducibly placed down on the center of the bar.

Somehow we wanted to attach the radioactive source to the movable metal plate on the scanner. The source sat in a cylindrical holder (See Figure 3.3) which in turn was bolted to the metal plate. The cylindrical

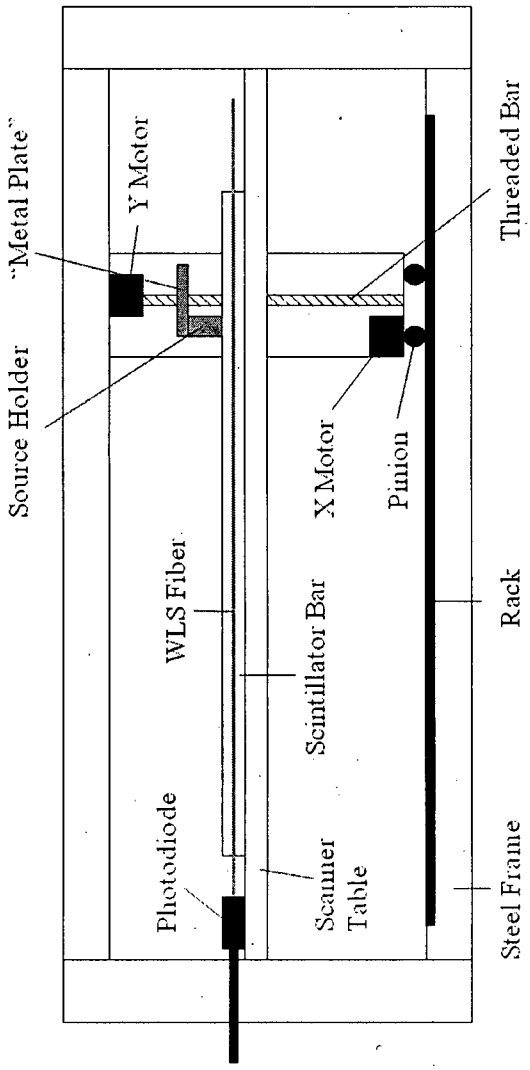

Figure 3.2: Schematic Diagram of the Bar Scanner

holder basically came in two parts: one, the outer part, remained stationary with respect to the metal plate and two, the inner part (dashed edges in the figure), could move up and down. The source itself was mounted to the bottom of the sliding part. The point of this sliding was to insure the source was always touching the bar even if the dimensions of the bar change as you move along a bar or from bar to bar. The down position of the scanner would be set so that the source would be pushed up slightly (1 cm or so). Therefore if another bar to be scanned is narrower or wider (by up to 1 cm) the source will still sit on the bar. If one bar didnt happen to be square the source may not sit flush with the side of the bar. To overcome this, part of the sliding section of the source holder is coupled using a piece of rubber tubing. The rubber tubing bends easily under the weight of the sliding part to sit flush on the side of the bar; however, the tubing is stiff enough so that if the bar is square the tubing will not bend.

As the scanner moves in the x-direction we believe that the source is reproducibly placed down on the center of the bar. The was no mechanism built into the scanner for checking this we simply always check that the guidance bar is always pushed up against the bar being scanned and we trust that the source holder doesn't move sizeways (perpendicular to the bar axis) on its path along the bar.

3.7 Threading a fiber into a bar

We had many discussions/thoughts as to how we would thread a bar onto a fiber. The problem with our smaller setups was that even with the utmost care the fiber would still bend before it went into the bar and it would pick up very fine cracks. We wanted a way to keep the fiber taut so that the bar could slide onto it without the fiber bending.

We had the idea that an approximately 1mm diameter straight metal wire could be placed inside a bar prior to it being placed on the scanner table. Once the bar was placed on the table the wire could be coupled somehow to the fiber, some tension could be put on the wire/fiber to pull them both straight and into alignment and then the bar could from the wire on to the fiber.

Another idea was to use a fiber much longer than the length of the bar. The scintillator bar is approx 2 meters so a piece of fiber about 4.5 meters could be used. First you slide the bar onto the end of the fiber so that it just comes through the far side. The part of the fiber that the bar covers in this position is ok to damage as it wont be transporting any of the light

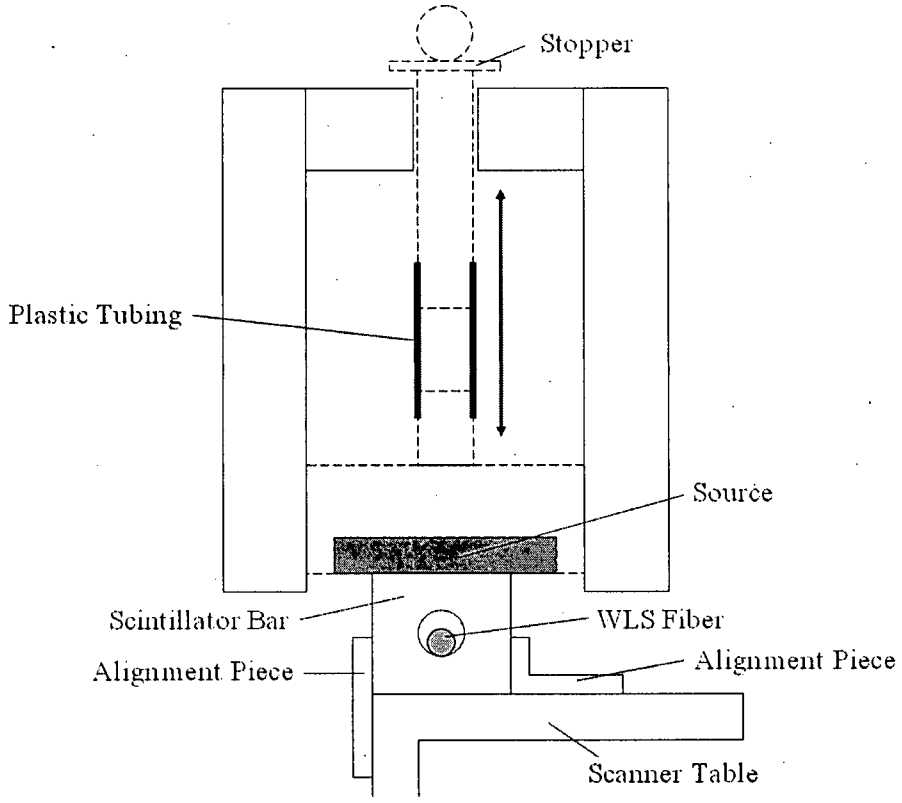

Figure 3.3: Schematic Diagram of the Source Holder setting the source on top of a Scintillator Bar. The two alignment pieces form the edges of the guidance trough

that is going to be detected. The end of the fiber could be taped down to the table so there is some tension in the fiber and then the bar could slide from this throwaway part of the fiber onto the good part of the fiber.

In the end we found that the little guidance trough (the trough formed between the two alignment pieces) for the bar worked well for keeping the fiber reasonably straight. Within the trough the fiber could only bend by a little amount and it was essentially straight as the bar passed over it. The bar could also be threaded onto the fiber quickly and smoothly. We used a 2.2 m length of WLS fiber for scnner and not the idea of using a much longer fiber.

In addition a few pieces of rubber tubing were placed around the fiber between the end of the bar and the photodiode. This part of the fiber was out of the bar's guidance channel and so could bend here. The rubber tubing stops the fiber from doing that.

3.7.1 Handling of the Scintillator bars and WLS fibers

So that grease from your hands wouldnt be transferred to the scintillator bars or the WLS fibers all handling was done wearing white cotton gloves.

3.7.2 Polishing the fiber

We have a fiber cutting device at TRIUMF. It essentially is made up of two parts: A diamond cutting blade which can be moved in and out using a stepper motor and a clamp for the fiber so it can be held in place whilst the diamond blade cuts it. For the most part, the cutting machine produces a very uniform smooth surface; the only problem is it leaves a few wispy hair-like pieces of plastic on one side of the cut. These can be simply removed using some tweezers however it is a time consuming step. For use on the scanner both ends of the fiber were polished.

3.8 Modifications to the room

A double side access door was closed and taped up with black electrical tape to keep out the light from the adjacent room. A black curtain maze was also erected to close off the aging test setup and scanner setup from the computer controls which were by the door of the room.

The WLS fibers peak response is to the ultraviolet end of the spectrum. Previous fibers worked on at TRIMF had been seen to age (produce less light) rapidly they were exposed to UV light. I covered all the florescent

lights in the dark room with UV filters (UV-opaque mylar. Named "Encapsulite Window Filter Weatherable Mylar" from Fuji Graphics Systems) so that when the lights were on to do work on the bars/test setup the fibers wouldnt get the UV exposure they might have. Later we decided to block out all wavelengths we thought the fibers were sensitive to so we added a red filter (Red Filter from West Coast Stage Lighting) to the florescent lights so that only red light could get through. It was noted that even with both these filters on the florescent lights the fibers were still excited by the light and you could see light come out from the ends of them.

3.9 Control of the motors/source position

The Scanner is controlled through a computer terminal with MIDAS as the interface between the user and the state of the scanner. The Scanner is run through 3 different programs; feMotor controls the motors, feBar controls the bar code scanner and feScan controls the Keithley Picoammeter. The user of the scanner essentially has control over the following parameters:

- Starting x position
- Starting y position
- y distance the source lifts from the bar between readings
- Jump in the x direction between readings
- Total x distance to scan over

In recent runs where we are more concerned at looking for the light yield of the bar rather than for small dead spots within the bar. We therefore only took three to four readings per bar so the jump in the x direction between readings was of the order 50 cm. This obviously increased the speed of a scan, doing the scan in 2 cm jumps will take of the order 5 mins with just a few readings it will take about 10 seconds.

3.10 Bar Scan Routine

Before scanning starts the startup procedure is,

1. Screw Ru-106 source into the source holder

2. turn on the Keithley Picoammeter. If the Photodiode isn't attached, press the ZC button and then connected it.

3. Start feMotor, feBar and feScan programs

4. Setup the previously listed parameters

Now each bar can be scanned following the procedure

1. Put a new scintillator bar on the fiber. Note: the first scan of each day should actually be done on the scintillator test bar (bar number 2 in out barcode labeling system). So for the first scan just leave that bar in place. (NB: We scanned the reference bar twice each day, at the beginning and end of each shift. We did this because there were daily fluctuations in the light output of the bar/fiber/photosensor setup which we didn't understand and so we divided out these changes by having a reference bar.) See the next chapter for a discussion of the systematics.

2. Scan the bar code on the scintillator bar with the bar code reader.

3. Go back to computer area. Turn off the lights in the dark room.

4. Start the scan

5. The plotted results shows the current as a function of position of the source on the bar. The graph for each bar is fit by an exponential (See Equation 3.1). The bar is characterized by the normalization (I_0) and attenuation length (x), and chi-squared of the fit. Write these results in log book, along with the bar code number. Also note if the fit looks good.

6. Decide whether a bar fails. The condition for failure are

   $\rightarrow I_0 < 5.0pA$, $\rightarrow x < 4000mm$, $\rightarrow chi > 3.0$.

   If the bar fails any of these conditions, put the bar in the "failure" pile. Also, make a note of it in logbook and explain why it failed.

7. Turn the lights back on.

8. Remove the scintillator bar from fiber and then start the procedure again with the next bar.

9. At the end of the day scan the reference bar again.

3.11 Bar Scanner Results

Figure 3.4 shows the data points for a typical scan. The x axis is the position of the source on the bar. Zero on the x axis is the far end of the bar from the photodiode, going more negative is getting closer to the photodiode and more positive is moving off the bar away from the photodiode. Data points are taken every 2 cm and are fit using the function,

$$f(x) = I_0 \exp(-(x + 2000)/x_0) \tag{3.1}$$

where I_0 is the current, in pA, when the source is at the near end of the bar and x_0 is the attenuation length, in mm, of the bar. The χ^2_{dof} is calculated using the usual χ^2 equation,

$$\chi^2 = \sum \frac{(y - y_i)^2}{\sigma^2} \tag{3.2}$$

here y_i are the value of the current for the data points, y is the value of equation 3.1 at that point, and σ is the error in each point, set to be 0.1pA. The error of 0.1 pA was estimated from the typical spread of the baseline noise. To get the χ^2_{dof} from the χ^2 you simply divide by the (number of data points - number of fit parameters).

Some observations of note from a typical scan are:

- The dashed line in the lower right hand corner shows the background current from the photodiode when the source in not sitting on the bar (around 0.5 pA). For analysis (i.e. fitting the Eqation 3.1 to the data) this baseline was ignored.
- The current doesnt jump from the background 0.5 pA to the best fit curve suddenly (mentioned in the next section).

At the beginning and end of each day a scan is done of a reference bar (bar 2 on its barcode). Each I_0 parameter for each bar is normalized by the I_0 for the reference bar on that day. The reason for this normalization was, due to there being daily fluctuations in the light output/light detection of the setup which we couldn't pin down, to divide out these fluctuations.

Figure 3.5 shows the I_0 for the bars run through the scanner already. This contains the 4 - 10 bars scanned from every box (approximately 100 bars) once it had come back from CELCO. The figure also contains the start of scanning 1 in 4 bars of the entire production run. The denser bands of vertical points in the figure are the boxes where 1 in 4 of the bars has been

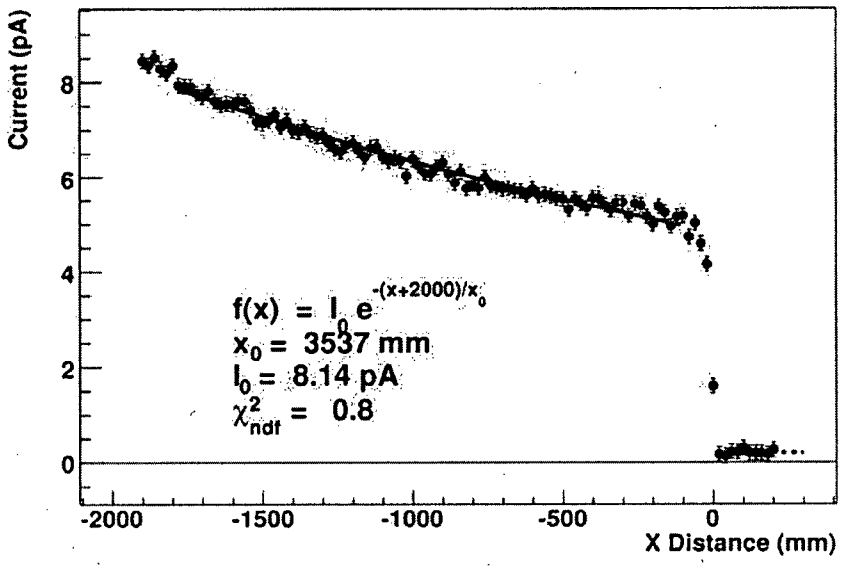

Figure 3.4: Example Scan

scanned. In the end we aim to scan 1 in 4 bars of the entire production run before they are glued into x-y layers.

The kink in the middle of this data at bar number 7500, originally thought to be related to the change of fiber-photodiode coupler, is thought to be real, perhaps related to an increase in the width of the bars as seen by the width measurements made during the production run. Around bar 9000 there is also a dip in the performance of the bars. There are more data points around this area as we wanted to find the full extent of the problem. The dip was over a few bars and those can be put to one side and not used in one of the xy layers.

Figure 3.6 shows a histogram of the normalized I_0 values for the measured bars. Even with the kink at 7500 the distribution is still remarkably Gaussian and even with the dip at 9000 the RMS spread of the data is only 5%.

3.12 Further tests with the bar scanner

Looking at Figure 3.4 around x = 0 shows there is not a sudden jump in the light output of the bar but is more gradual over a few cms. There are two

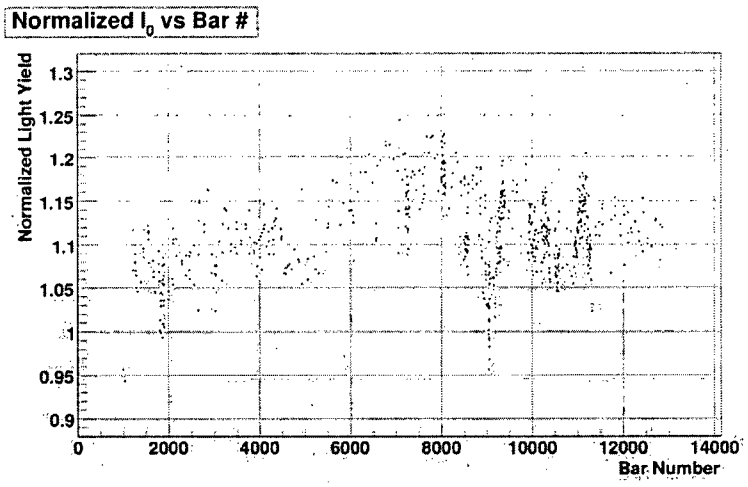

Figure 3.5: Normalized Light Yields vs. Bar Number

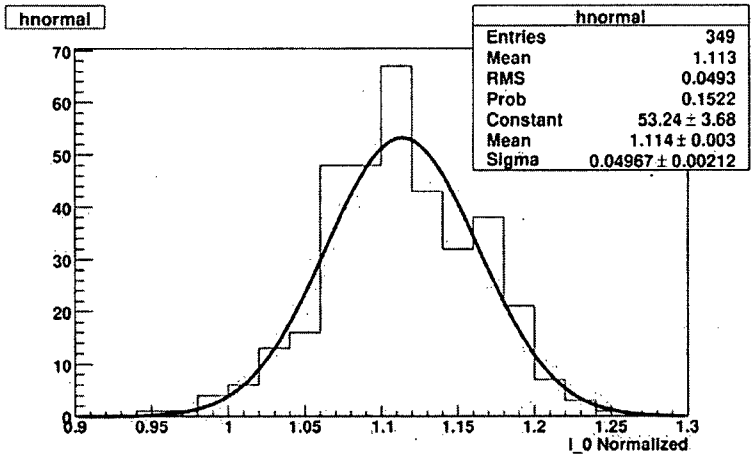

Figure 3.6: Distribution of Normalized Light Yields

possible mechanisms for this; either electrons from the source come out of the end of the bar and don't deposit as much energy and/or light scintillated near the end of the bar comes out of the far end of the bar and doesn't get into the WLS Fiber.

To separate these two possibilities I decided to paint the end of a bar with very reflective white paint (Avian White, from Spectrum Coatings Inc.) and scan it and compare it to an unpainted bar. Figure 3.7 show the result of two scans; one with the end of the bar painted white and one without. The data for the bar with the painted end still doesnt jump suddenly at the end of the bar and so this must be due to the electrons escaping out the end of the bar. For further analysis of the effect of white paint I took the ratio of the two data sets to and produced Figure 3.8. This shows that painting the ends of the bar only makes a difference over the last 4 cms with only approximately a 10 % difference in the light yield if a particle were to go through the bar in those few cms. We decided that this 10 % difference over the last few cms was not worth the trouble of painting all of the bars.

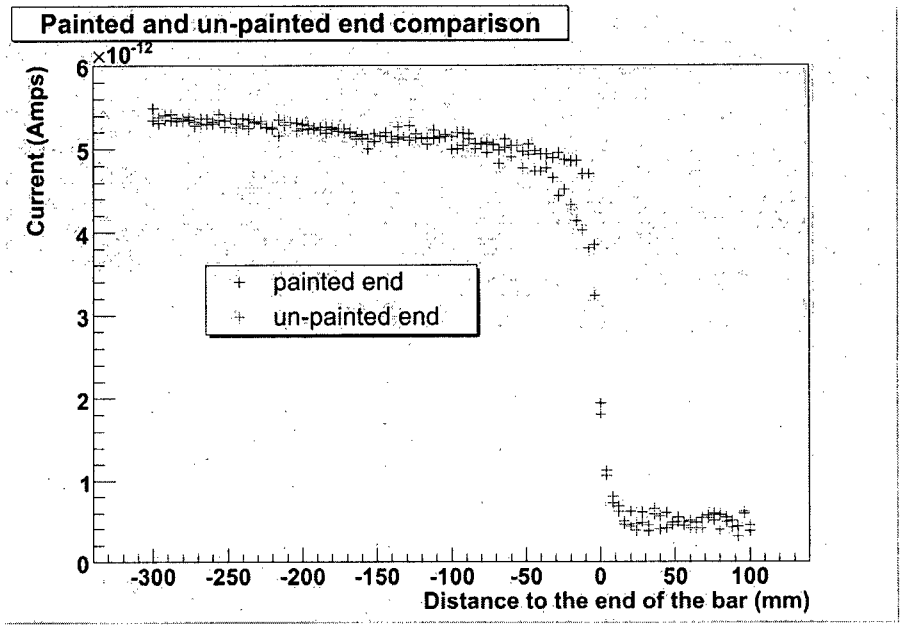

Figure 3.7: Bar scan of the end of two bars. one with its far end painted white and one without. Results were taken with two bars to avoid the poorly understood daily fluctuations. The current from one of the bars was scaled so the data overlaps and the effect of a painted end is isolated.

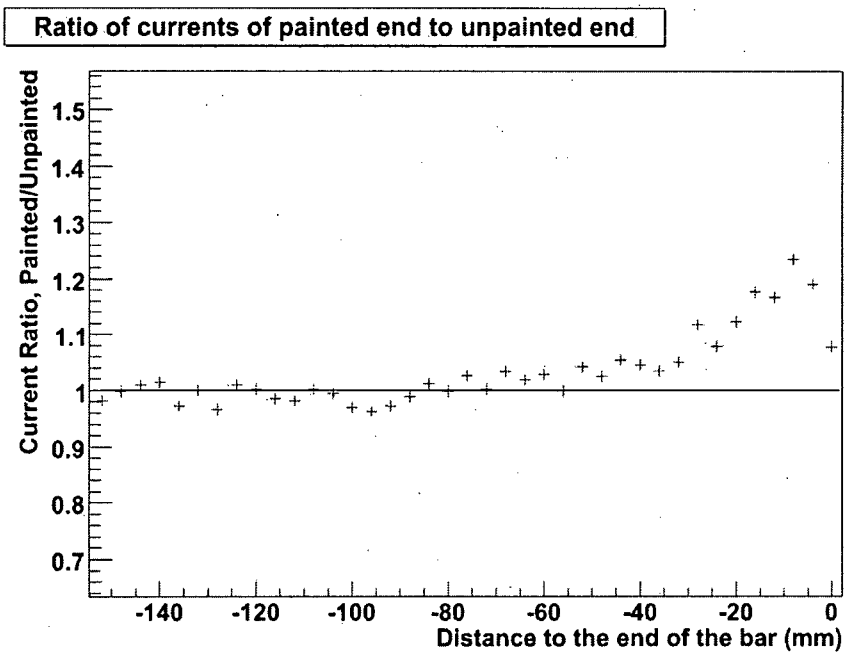

Figure 3.8: Ratio of a scan of a bar with its end painted white to one without paint

Chapter 4

Aging Studies

4.1 Introduction

From previous beam tests carried out in early 2006 a measurement was made that suggested that our bars were aging (i.e. their light output had decreased over time). The observed aging rate was significant enough for us to pay attention to it and one which we should measure/characterize properly. If the aging was due to a chemical reaction happening in the bar the aging rate could be speeded up by storing the bars at higher temperatures. Such a change in rate as a function of temperature can be described by the Arhenius equation.

$$k = Ae^{-E_a/RT} \tag{4.1}$$

This expression shows the dependence of the rate of a reaction k on the temperature T (in Kelvin), the activation energy E_a, the gas constant R and a prefactor A. The activation energy E_a , in our case, is the energy threshold for active scintillator to turn to dead scintillator. The units of k are the same as the units of A which would typically be s^{-1}. For my purposes days^{-1} is a convenient unit for k as will be shown later.

Measuring the aging rate, k, at two different temperatures (higher than room temperature) would be enough to solve this equation for our scintillator and then we could predict the aging rate when the bars are stored at room temperature (i.e. whilst they are being stored, glued into x-y modules, fitted into the FGD and finally in the experiment itself).

The aging rate of the scintillator at room temperature was thought to be fairly low; therefore, trying to measure the rate directly would take a long time and would need to extremely accurate. The plastification point of our polystyrene plastic is around 90-100 degrees Celsius so we couldnt heat the bars up this high. We chose to store two sets of bars at different temperatures, 60 and 85 degrees Celsius

4.2 Aging Setup

I set up the test setup as follows. The copper pipe with the photodiode in it was taped down at one end of the table. A 30 cm piece of WLS fiber, cut perpendicular at both ends with the fiber cutter was glued into the acrylic piece on the end of the photodiode with some 5 minute epoxy. The epoxy was used to assure the same fiber-photodiode coupling for every measurement. If the fiber is allowed to move in and out or rotate with respect to the photodiode the results would be meaningless to what we are trying to understand.

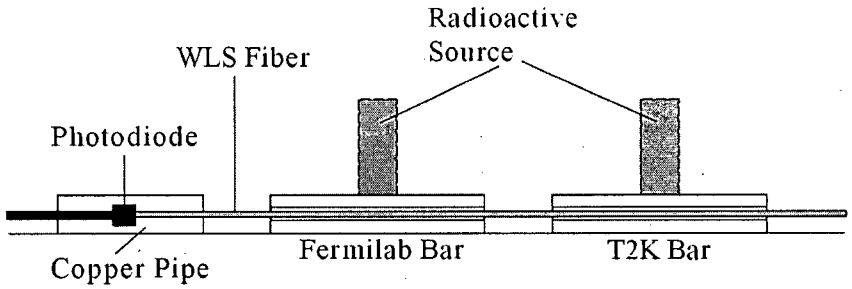

Figure 4.1: Aging Test Setup. The dashed rectangles show where the Sr-90 source is place on the bars. The Fermilab bar was not in the original accelerated aging study but was added later as a reference.

To improve statistics we chose to cut 10 bars, of length 10 cm, to be stored at 85 degrees and 10 bars, of length 10 cm, to be stored at 60 degrees. Each bar had a point marked on it, in the center of the bar (with respect to the sides and the length) so the Sr-90 source is placed down on the dead center of the bar.

The top of a 15 cm deep cardboard box was cut off, it was made light tight on all the other sides with electrical tape and a 4 inch wide black felt skirt was taped around the open side of the box so that this open side could be the bottom and the whole box could be placed over the entire setup. A piece of tape was put down the far side of the box as a hinge so the box could be carefully raised and lowered.

The 85 degree bars were stored in a digitally controlled oven and we were confident the temperature remained stable. The 60 degree bars were stored in an oven which had very little control and took a long time to stabilize its

temperature.

Before the bars were put in the ovens for the first time readings were taken to see how much light they produce. Later when you wanted a reading to be taken the bars would be taken out of the oven and given 30 minutes to cool down. Hotter bars gave more light and took 30 minutes to stabilize at their room temp outputs. Once the readings had been taken (this happened at 11 am on each measurement day) the bars were put back in the oven.

4.3 Data Analysis

Each bar starts off with its own unique light yield.

1. Each Bar is normalized to its light yield on day 0
2. The average of the normalized values of all 10 bars is computed for each day's data.
3. The SD of these normalized values is found.

These aging rates for the bars came out much higher than expected (maximum of 2% as measured by Fermilab on the SciBar scintillator bars) and projecting the rates to find a room temperature rate gave an astonishingly high aging rate, as seen below:

Assuming

$$I = e^{-kt} \tag{4.2}$$

where the rate, k, is given by the Arhenius Equation

$$k = Ae^{-B/T} \tag{4.3}$$

With $k_{60^\circ C} = 0.01325 \pm 0.00147$ days^{-1} and $k_{85^\circ C} = 0.02328 \pm 0.00090$ days^{-1}. Solving to find A and B and extrapolating to find k at 20 degrees gives

$$k_{20^\circ C} = 0.00440 \pm 0.00008 \text{ days}^{-1} \tag{4.4}$$

or equivalently 3% loss of light output in a day, 75% in a year.

On further discussions with Fermilab (the guys that gave us the scintillator recipe) we decided that 85 degrees was way too close to the plastification point for comfort and we should do accelerated aging at lower temperatures.

As we only had one oven that was stable enough to trust we decided to start up the test with 10 bars, 10 cm long to be stored at 45 degrees and have 10 bars to be stored under normal conditions at room temperature.

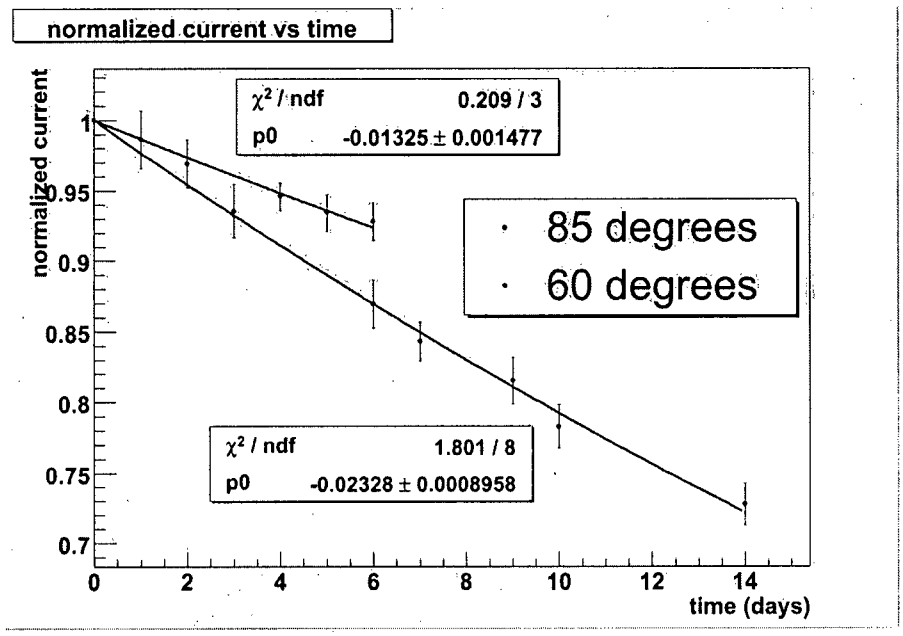

Figure 4.2: Normalized Current (Light Output) vs. time for bars stored at 60 and 85 degrees Celsius

Figure 4.3 shows the raw data for these bars over a 295 day period. Raw in the sense that each bar has been normalized to its light yield on day zero, and then averaged. The error bars are the standard deviation of the normalized values. There hasn't been any correction for the decay of the strontium source at this stage. The Fermilab bars were added on day 44 and were used as a reference bar as their aging rate was said to be understood. I will mention this in a later section. The Fermilab bars could also be used to cancel daily changes in the light output that we didn't understand.

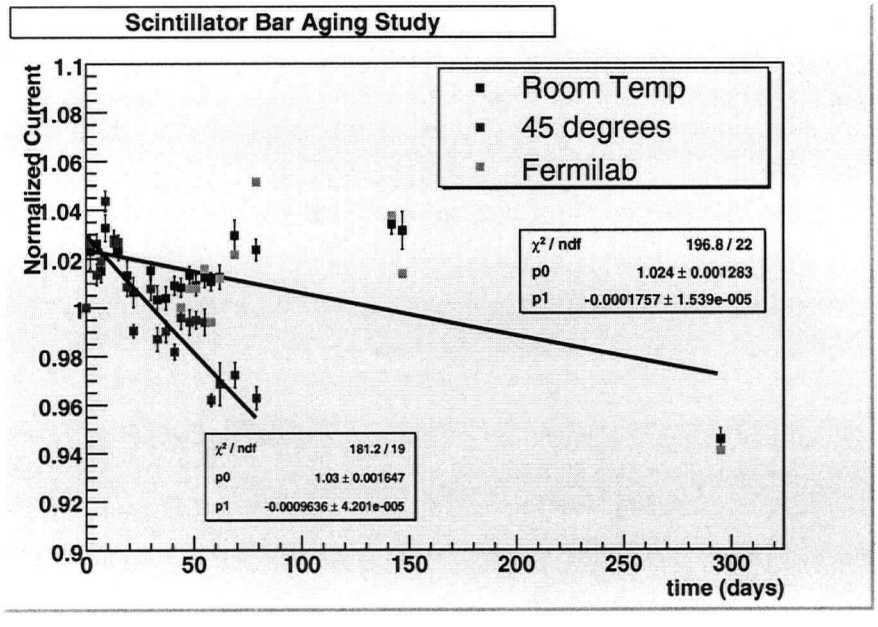

Figure 4.3: Normalized Current vs. time for FGD and Fermilab bars stored at room temperature and FGD bars stored at 45 degrees Celsius

4.3.1 Daily changes in light output

There were daily changes in the light output of the bars. We thought that this might be due to daily changes in temperature/humidity down in the basement. We monitored these two quantities for a month or so and saw no correlation between them and the light output of the bar. Sometimes when a photodiode was connected to a photodiode it took a few days for the noise rate to decrease and stabilize at an acceptable level. Why this occurred was poorly understood. Problems related to changes in the light output were put

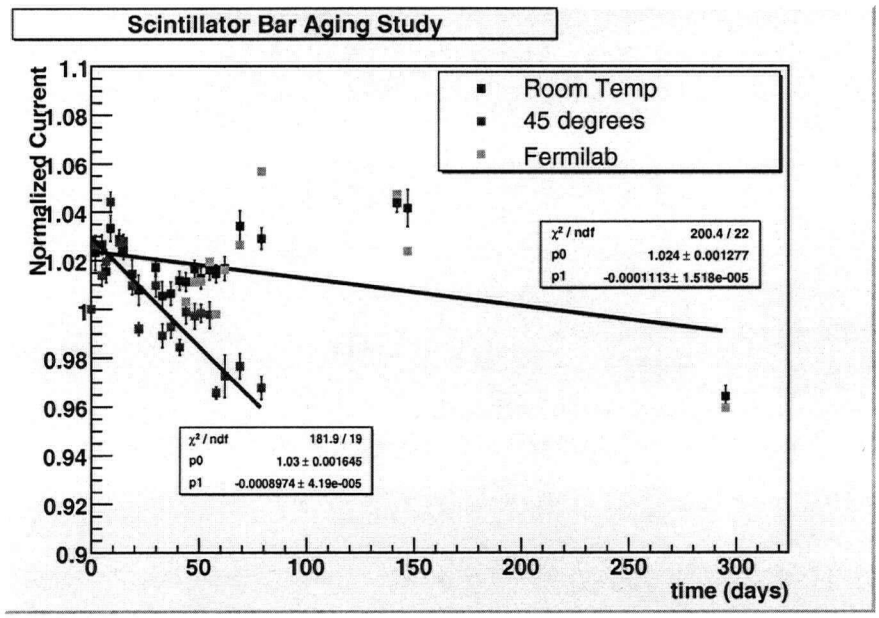

Figure 4.4: Normalized Current vs. time for FGD and Fermilab bars stored at room temperature and FGD bars stored at 45 degrees Celsius. The data points have been corrected for the effect of the source activity decreasing.

down as systematic uncertainties. I will now try to estimate the uncertainty in the measurements due to these systematics.

The first change to the data in figure 4.3 was to correct for the decreasing activity of the strontium source (strontium has a 29 year half-life). Making this change reuslts in figure 4.4. The difference between Figure 4.4 and Figure 4.5 is the size of the error bars. Figure 4.4 has just the statistical or standard error bars, for the room temperature bars and the 45 degree bars, calculated from the spread of the 10 bars. Due to the daily fluctuation in the light output the χ^2_{dof} is huge. This indicates an additional systematic that wasn't controlled for. The Particle Data Book [10] recommends, in order to get an idea of the unknown systematics, to increase the size of the error bars until the $\chi^2_{dof} = 1$. To get the χ^2_{dof} down to around 1 I needed to triple the size of the error bars. The typical statistical errors for the data points were around 0.005 and so the typical systematic errors are around 0.01 for the data points. Consequently the errors returned by the ROOT fitting program for the fit parameters change. The aging rate of the room temperature can be read off Figure 4.5 to be $k_{\text{room temp}^\circ C} = 0.00011 \pm 0.00005$ days^{-1}. This is equivalent to 0.01 % per day or 4.06 $\pm$ 1.6 % per year.

4.3.2 Adding SciBar scintillator bars

Scintillator produced from the same recipe as ours was made at Fermilab for the SciBar experiment. They were confident that their scintillator aged at a rate below the 2 percent level [11]. We decided to add a Fermilab bar to our setup for comparison with the room temperature stored bars. The Fermilab bar was added on day 44. Since these bars have been added to the setup it is clear that the light outputs of Fermilab bars and our scintillator bars track each other and if you plotted the ratio of the two as a function of time you would get a flat straight line (See Figure 4.6). Fitting the ratio with an exponential gives a separation rate of $k_{\text{separation}} = 0.000005 \pm 0.000058$ days^{-1}. This is completely consistent with zero and therefore we are confident that our bars, if they age at all, age at a rate similar to that of Fermilab bars; i.e. less than 2 percent decrease in the light output per year.

A rough empirical law for scintillators it said that for every 6 degrees Celsius increase the aging rate will double. If I take the aging rate of the 45 degree bars from Figure 4.5 I get $k_{45^\circ C} = 0.00088 \pm 0.00013$ days^{-1}. Using the scaling rule,

$$k_{45^\circ C} = 0.00088 \pm 0.00013 \text{ days}^{-1} \tag{4.5}$$

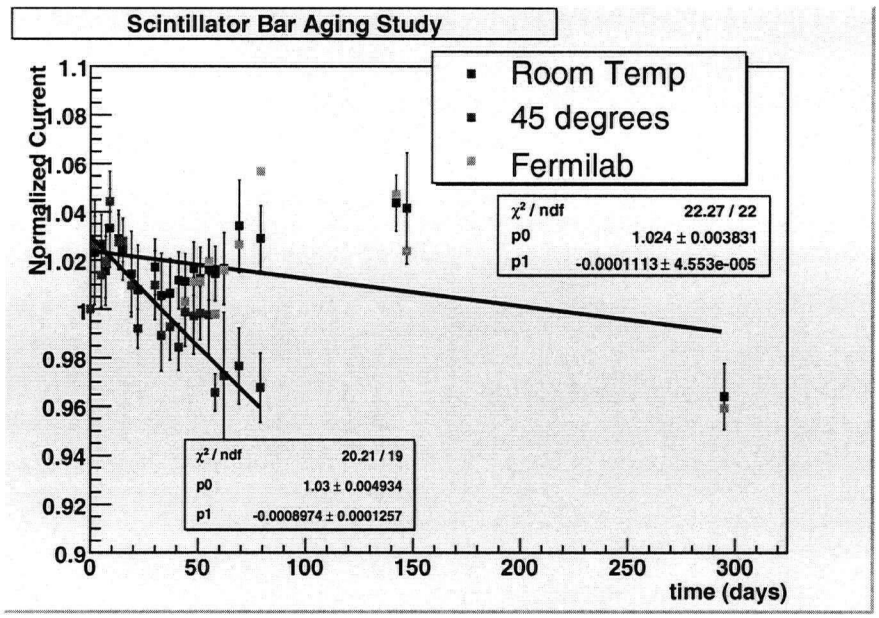

Figure 4.5: Normalized Current vs. time for FGD and Fermilab bars stored at room temperature and FGD bars stored at 45 degrees Celsius. The data points have again been adjusted to account for the activity of the source dropping over time. The error bars have also been increased so as to give a χ^2_{dof} of around 1 and then the increase will be a good measure of the systematic errors.

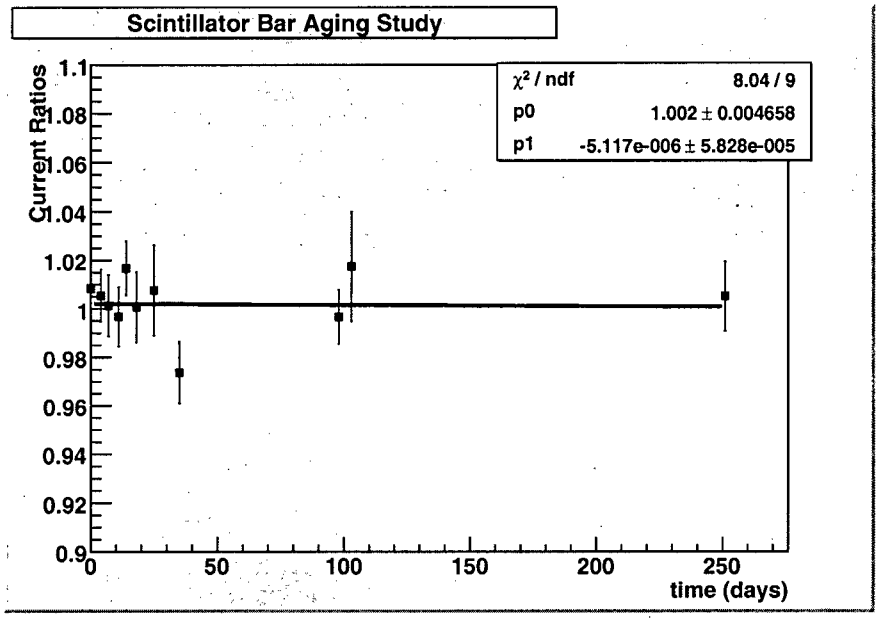

Figure 4.6: Plot of the ratio of the room temperature bars to the Fermilab bars (also stored at room temperature). Note that day zero on this figure corresponds to day 44 on the previous 3 figures.

therefore

$$k_{20°C} = \frac{k_{45°C}}{2^{(45-20)/6}} \quad (4.6)$$

$$= 0.000048 \pm 0.000007 \text{ days}^{-1} \quad (4.7)$$

or equivalently 1.93 ± 0.25 % per year. A much more comforting number.

4.4 conclusions

We are left we 4 results to interpret/trust. These results are:

1. The 3% loss of light output in a day or 75% in a year result from scaling the 60 degree and 85 degree aging rates.
2. The 3.93 ± 1.60 % per year direct measurement from the room temperature data in Figure 4.5
3. The 1.93 ± 0.25 % per year prediction from using the scaling rule to the 45 degree data in Figure 4.5
4. Fermi labs bars have been measured confidently to age at less than 2% per year. A separation between the light output of our bars a room temperature and Fermi labs bars at room temperature over a 250 day period is consistent with zero. From the error in the slope of Figure 4.6 we can write down an aging rate for our bars of 2.0 ± 2.1 %

The first result was thrown out very early as we were going too close to the scintillator's plastification point for comfort. Also the applicability of the Arhenius equation to the problem in hand was questioned. The second result is attractive as it is the only direct measurement of the aging rate. Results 2, 3 and 4 are entirely consistent with each other and these are the results we trusted when deciding to go ahead with the full production run of the scintillator bars.

Chapter 5

M11 Beamline Results

5.1 Motivation

In December 2006 we did a 2 week run using the M11 beam line at TRIUMF. The motivation for the beam test was to test the new MPPCs against the Russian Silicon Photomultipliers, measure the crosstalk rate for the MPPC for different bias voltages, start an aging test on more than one bar in a controlled way to be tested again in the future and to measure the absolute light yield from the scintillator.

5.2 Beam Test Setup

Nine bars were chosen to be tested in the beam. eight of these were bars produced in May 2006 and the other was produced in November 2006. We decided to put them in a vertical stack, four May bars on top and the bottom with the January bar in the middle (See Figure 5.1 for a diagram of the setup).

We had done previous measurements of crosstalk between bars due to light passing through the TiO_2 coating before so this time we wanted to optically isolate each bar. This was done by putting a piece of Tedlar, which ran the entire length of the bars, under one bar, over the next, under the next, and so on. A further piece of Tedlar was wrapped around the entire bundle of bars to keep light out; only a couple times around the bars makes a light tight maze which is sufficient to keep the light out.

For a solid surface to hold the bars above we used a 2 inch wide (also well over 2 m long) steel U channel. To hold the bars at a fixed height above the U channel 2 approx 2 inch high wooden shims were put under the bars. To keep the 9 bars vertical polyethylene was cut using a utility knife and then placed around the bars next to the wooden shims.

We had previously done tests to measure the reflectivity of various reflectors on the end of the fiber so this time we did without reflectors. Further to ensure next to no reflection from the far end of the fiber we cut the ends

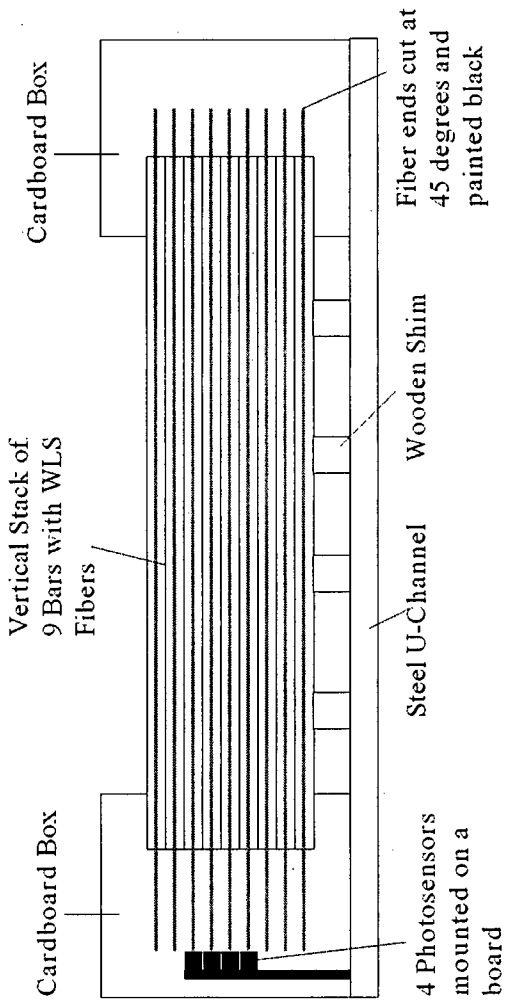

Figure 5.1: M11 Beam Test Setup Schematic

using a razor blade at a 45 degree angle with respect to the fiber axis and we painted the ends black using standard matt black paint. The readout ends of the fibers were prepared in the usual way, being cut with our automated diamond cutting blade.

To cover up the far end of the bars we used a small cardboard box (approx 1ft cubed). A U shape was cut from both ends of the box so it could be slid onto the U channel. A 9 cm by 1 cm hole was also cut on one side of the box so the bars could be slid in. To insure that light couldnt get through this 9 cm by 1 cm hole a thin flexible black plastic was made to be a collar around the bars next to the hole. This collar and the 2 U shaped holes were taped up using electrical tape to make them as light tight as possible. The box was also painted black on the inside to absorb any stray photons that would get into the box. An access hole was cut into the box on the opposite side to the hole the bars come in through. This was so that, if needed, fibers could be pulled out of the bars and through the end of the box and then replaced.

The readout end of the bars was slightly more complicated. A similar size box as used on the other end was prepared in exactly the same way as before (2 U channel sized slots and one 9 cm by 1 cm hole with collar, painted black on the inside and taped with electrical tape to make light tight). The photosensor-fiber couplers were the same as used for the aging test and the early bar scanner coupler, the only difference being that the fibers weren't glued to the coupler.

4 photosensors (3 Russian SiPMs: Serial numbers 76, 93, 105 and 1 MPPC: Serial number 400) were connected to a small board (used to feed the bias voltages to the photosensors) which was held to the U channel and box using 2 cable ties.

5.3 Beam setup

The momentum of the particles coming from the M11 beam line at TRIUMF is selected by setting the various magnets to pre-determined values. In our beam test we did runs where we had the particles at 120 MeV/c and 400 MeV/c momentum. A trigger counter, with dimensions 1.3 cm wide by 4 cm tall by 4 mm thick, was placed just between the end of the beam line and the 9 Bar Setup and trigger counter, with dimensions 15 cm wide by 15 cm tall by 12.5 mm thick, was placed another 4.4 meters downstream. The trigger counters were used for two reasons;

1. When both of the trigger counters are triggered within a certain small

time window (approximately 20 ns) it is assumed that the same particle has caused both the hits and has therefore came from the beam line and has the correct momentum.

2. The time difference between the two hits on the trigger counters is recorded and then this can be used to separate the different particles. The electrons being the lightest will cross the 4.4 m span in the quickest time up to the protons, being the heaviest, which will cross the span is the longest time. At 120 MeV/c momentum the time of flight separation between the particles is very efficient however the flux is low. We finished the run using 400 MeV/c momentum protons as the flux was much greater and runs could be shortened.

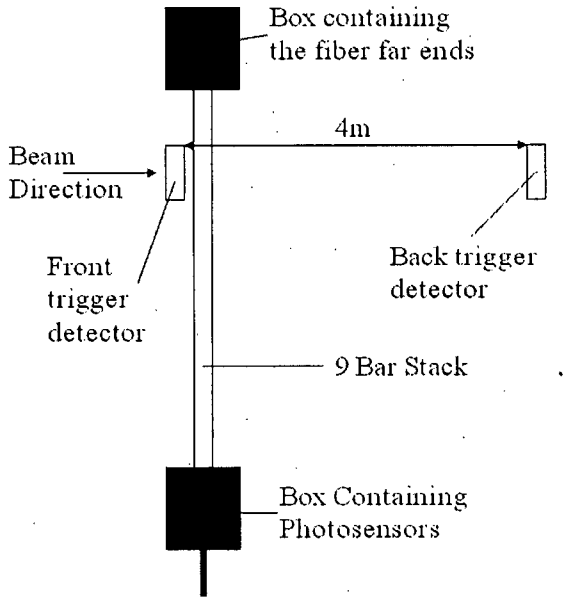

Figure 5.2: Top view schematic of the beam test area

5.4 electronics

The Trigger Counters were both read out using PMTs. The front trigger counter was at -1600 Volts and the back trigger counter was at -1800 Volts.

Signals were both fed into discriminators and if they were above threshold a standard NIM (-700 mV) square pulse would be sent to a coincidence counter. If the pulses happened within a 20 ns coincidence window a 250 ns gate was opened on the ADC connected to the MPPC so that the charge created in the MPPC by the particle passing through the trigger counters could be measured. A wide gate was needed because the output pulse from the MPPC photosensors had a longer tail than previous Russian SiPMs .

A second identical set of signals nim signals are put through delay lines and if the coincidence of the two particles is seen then a TDC will find the time between the 2 pulses for later use in the separation of the particles.

5.5 Data Taken

The was a limited amount of good data taken over the few day run period. There were a few setup runs, some calibration runs where we wanted a low light level so we could easily resolve individual photo peaks, some long runs using 120 MeV/c momentum e, μ and πs, and then some short runs using 400 MeV/c protons (See Table 5.1). As the run went on we had a few problems which cut down the amount of data we could gather. Two of the ADC channels died so by the time we were looking at MIPS we only had spectra from one Russian device and one MPPC. The second setup period came about because a preamp died and so we decided to switch the Russian device onto the only working channel remaining for the MPPC.

5.6 Calibration Runs

The purpose of the calibration runs was to find the gain of the photosensor as a function of bias voltage. The gain of a Silicon Photomultiplier is the distance between photo peaks in the charge spectrum. Similarly it is the slope of the straight line which goes through the points on a peak position vs. peak number plot.

To see the individual peaks in the photosensor charge spectrum low light levels are needed. To get this we decided instead of pulling the fibers back from the photosensor to pulse the far ends of the bars with an LED. A single LED was taped to the inside of the box at the far end of the bars.

I wanted an automated way of fitting the charge spectrum and extracting the peak position. I had two fits for doing this. One was to fit the entire spectrum with one continuous function and one was to fit the photo peaks individually (See Figure 5.3).

Table 5.1: Run summary

Run Numbers	Purpose	Beam	Photosensor	Beam Position
1781 - 1794	Setup	120 MeV/c e, μ and π	3 Russian SiPMs @ 45.5 - 47.5, MPPC @ 68 -71 V	195 cm
1795 - 1807	Calibration	120 MeV/c e, μ and π	2 Russian SiPMs @ 45.5 - 47.5, MPPC @ 68 -71 V	195 cm
1810 - 1824	MIPS	120 MeV/c e, μ and π	Russian SiPM @ 45.5 - 47.5, MPPC @ 68 - 71 V	195 cm
1825 - 1837	Setup	120 MeV/c e, μ and π	Russian SiPM @ 45.7V, MPPC @ 69.8 V	195 cm
1838 - 1875	Attenuation/Light Yield	400 MeV/c Protons	Russian SiPM @ 45.7V	50 cm - 195 cm

To fit the peaks individually, I first looked at the charge spectrum and picked ranges over which to fit Gaussians. This ranges isolated were the photo peaks but not the troughs.

For the continuous function I first counted the number of peaks in the charge spectrum and I fitted it with the sum of the same number of Gaussians. I would take the parameters of the individual peak fits and use these as input parameters for the continuous fit. I could then take the fitted parameters and plot the position of the Gaussians as a function of the peak number.

The next figure (Figure 5.4), which is zoomed in shows that the continuous function doesnt fit too well to the spectrum. The function doesn't fit the troughs well and in the effort to fit these troughs the fits are skewed to the left slightly. The individual peak fits don't include the trough and therefore seem to fit the peaks themselves, and therefore returns the position very well. Figure 5.5 is a plot of peak position vs. peak number using the fit parameters from the continuous fit. Originally I had used the errors, as returned by the fitting program [13], of the peak locations. When fitting a straight line to the data the χ^2 was obviously too large and so the error bars must have been way under estimated. A good estimate for the error on the peak location would be resolution of the ADC (i.e. the bin with for the ADC). Doing this I got a reasonable χ^2 of 8.714 for 5 degrees of freedom. Figure 5.6 is a plot of peak position vs. peak number using the fit parameters from the individual fit. Using the same error estimate as for the continuous fit I got a χ^2 of 13.31 for 5 degrees of freedom.

The data from the individual fits were used to produce Figure 5.7. This is a plot of the slope of the individual fits plots as a function of the different bias voltages tested during the calibration runs. It is true that the continuous and individual fits gave very close results for the gain. I decided to go with the individual fit results simply because the fit looked visually better than for the continuous fit.

Figure 5.7 shows the slope of the individual fit for different bias voltages for the MPPC. The errors in the slope of the individual fit graphs was used for the error in the gain. I believe there was also an error in the voltage supplied to the photosensor. The CAEN multichannel voltage supply device, had two values on the screen, an input voltage and a readback voltage and often there was a discrepancy between the two, of the order 0.01 - 0.02 volts. Putting in an error of 0.02 volts gives a reasonable χ^2 value of 6.075 for 4 degrees of freedom.

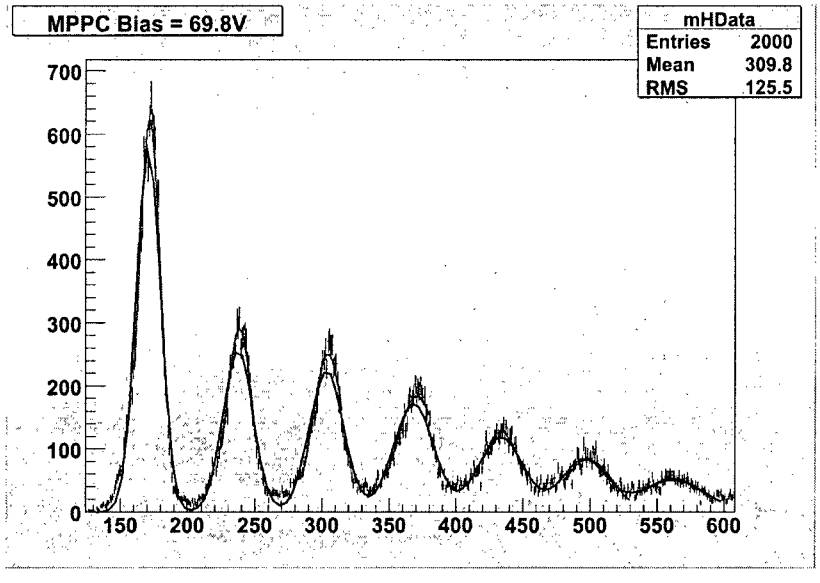

Figure 5.3: Example of a fit to a calibration run. The peaks are fit in two ways: The red curves are Gaussian fits to the individual peaks; The blue curve is a continuous function made out of a series of Gaussian functions.

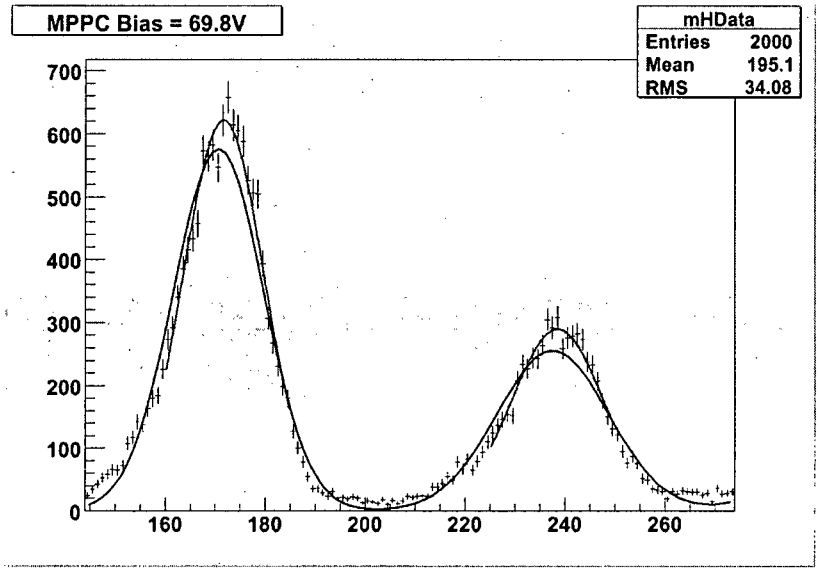

Figure 5.4: Zoomed in version of Fig 5.3. Shows that the continuous fit function (blue curve) has been dragged slightly to the left to by the more populous than expected troughs. The Individual peak fits (red curves) seems to fit the peaks well.

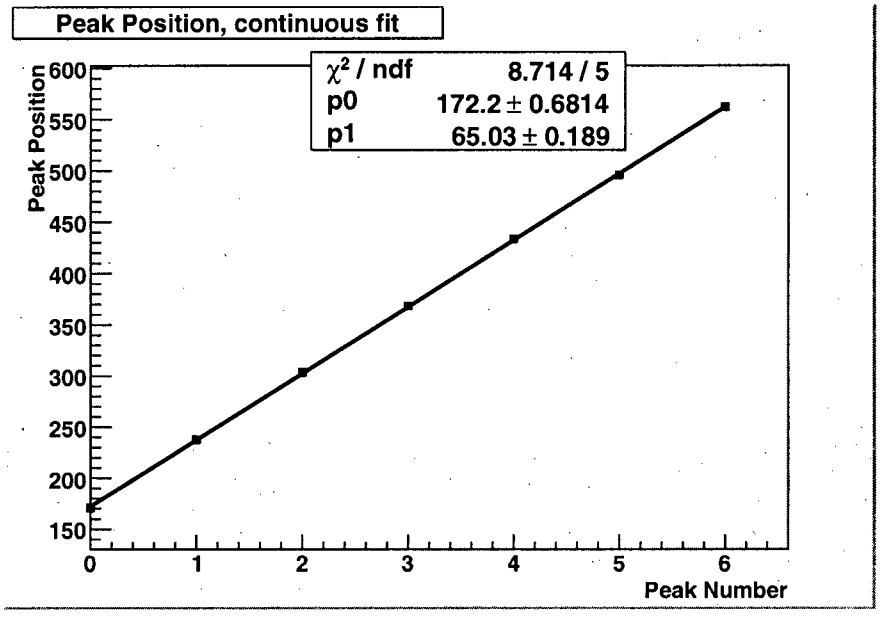

Figure 5.5: Peak position as a function of peak number using the fit parameters from the continuous fit. The function is fit with a linear function, the slope of which being the gain. The error in the peak position was chosen to be the width of one bin on the ADC. The errors returned by the ROOT fitting program gave very low error estimates and hence a very high χ^2

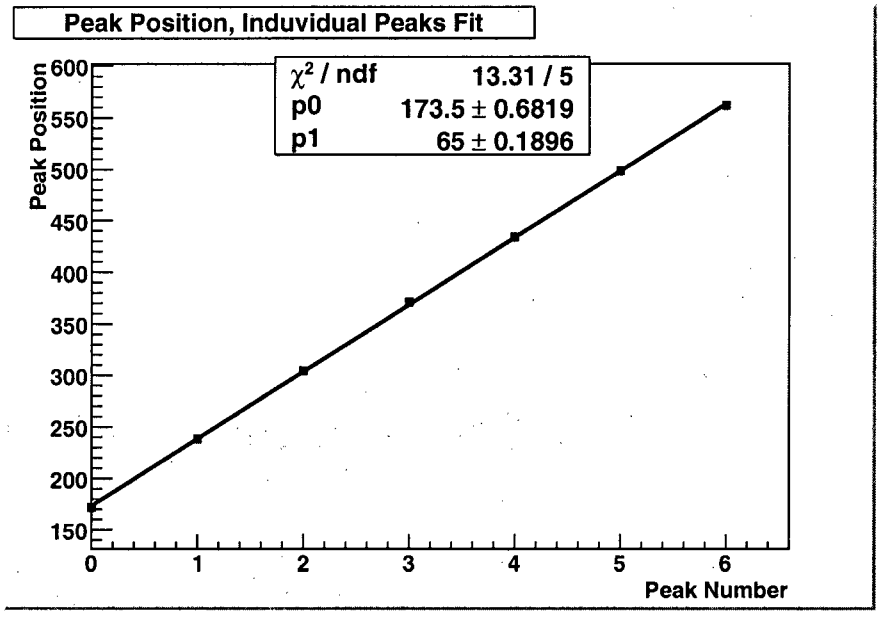

Figure 5.6: Peak position as a function of peak number using the fit parameters from the individual fits. The function is fit with a linear function, the slope of which being the gain.

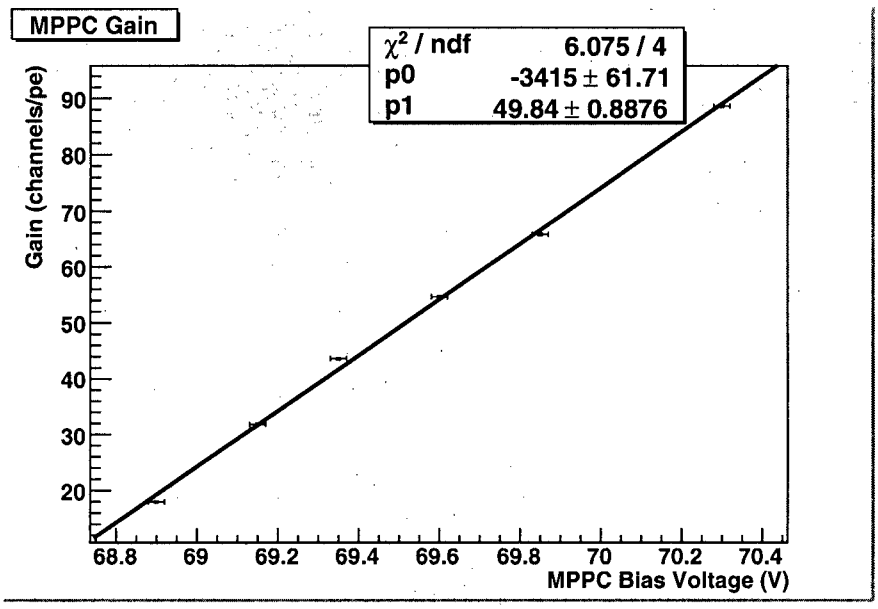

Figure 5.7: Gain as a function of voltage for the MPPC device. The Error in the gain is the error in the slope of 5.6 as returned by the fitting program. The error in the voltage is set to be the typical discrepancy between the input voltage and readback voltage on the CAEN supply. The y error bars are too small to see on the graph.

5.7 Crosstalk and Saturation Effects

From the beam results we would get numbers of photoelectrons that the photosensor, at different bias voltages, detects for different particles with different energies. From this number I wanted to predict how many photons actually hit the photosensor and how many are due to crosstalk and saturation.

5.7.1 Crosstalk

When a pixel fires inside the photosensor it can trigger a neighbouring pixel to fire. This happens when light from an avalanche passes across to a neighbouring pixel and causes an avalanche there. We assumed that a pixel only could fire a pixel directly touching the fired pixel (discounting diagonally touching pixels) and the probability of firing the neighbouring pixel is x. There are of course photosensor edge effects as pixels on the edge of the array of pixels will either have 2 or 3 nearest neighbours and not 4. There is a another effect similar to crosstalk which is called afterpulsing. Afterpulsing is where some of the electrons from an avalanche in one of the pixels get trapped. The can be re-emitted sometime later causing a pulse even when the pixel has recovered. I can't separate the two effects with my analysis so from now on crosstalk + afterpulsing is simply known as crosstalk.

5.7.2 Saturation

The photo sensors have a limited number of pixels, 400 for the MPPC used in the beam test. If a pixel fires, for a certain time afterwards, it will not fire again. Thus if two photons are incident on the same pixel at the same time only one of the photons will be measured.

5.7.3 Simulation

I made a simulation to simulate these effects so that you could throw a few photons at this device and then after crosstalk and saturation effects would give you the number of pixels that actually fired.

I programmed a 20 pixel by 20 pixel array each pixel being assigned a binary number (0 for not fired and 1 for fired).

5.7.4 Algorithm

- Randomly throw a photon at a pixel in the array

- If it has already fired stop here
- If not, fire the pixel
- If the neighbouring pixels havent been fired check if they fire using a certain cross talk probability
- Repeat for the desired number of incident photons

I took this code and ran it in a big loop, first over the number of incident photons and secondly over the value of the crosstalk probability x. For each incident number of photons I looped the code 1000 times so I could go ahead and calculate the rms spread of the number of photons detected. For each crosstalk probability I produced a graph of fired pixels vs. incident pixels. The graphs curved over to a maximum number of fired pixels of 400 at different rates, higher crosstalk levels plateaued quicker than lower cross talk levels.

These graphs were all linear for the first 30-50 incident photons so I fitted them all with linear functions from 0 to at least 30 incident photons (See Figure 5.10).

I took the slope of these graphs which I labeled at $(firedpixels/incidentphotons)_0$ and plotted them as a function of crosstalk (see Figure 5.11). The errors on the points are the errors in the slopes of the photons detected vs. incident photons graph. The $(firedpixels/incidentphotons)_0$ vs. crosstalk graph is fitted very well using a cubic function. I could then use this function from now on to find the average number of incident photons on the photosensor once given the number of fired pixels and the crosstalk parameter,

I also fitted these curves for different crosstalk values with saturating exponentials. The equation fitted was,

$$P_{det} = A(1 - \exp\left(\frac{-P_i}{B}\right)) \tag{5.1}$$

Where P_{det} is the number of photons detected, P_i is the number of incident photoelectrons if there were no crosstalk or saturation and A and B are free parameters to be fitted. A actually isn't a free parameter, it's the maximum number of pixels that could fire which is of course the total number of pixels, 400.

Without crosstalk B is equal to the number of pixels. Plotting B as a function of the crosstalk probability interestingly gave a linear graph. The saturation rate is thus inversely proportional to the crosstalk rate.

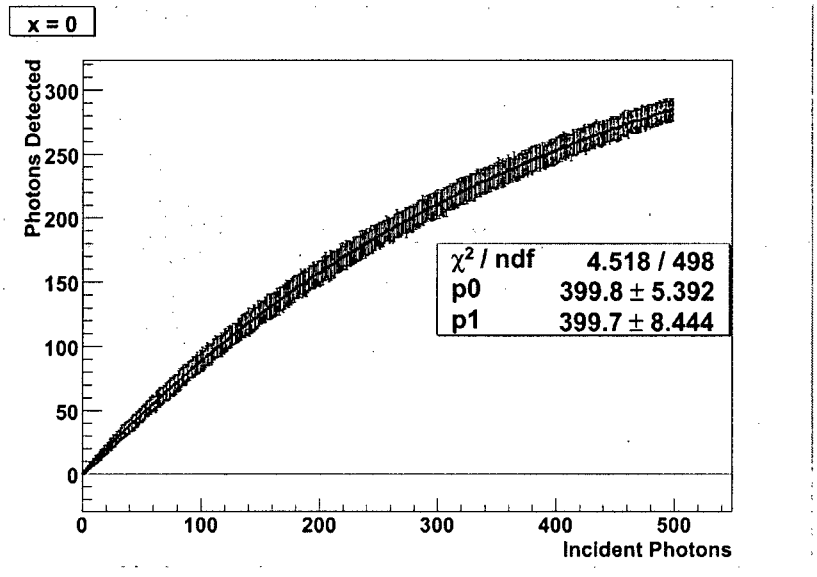

Figure 5.8: Simulated data of fired pixels vs. incident photons for a 400 pixel sensor without crosstalk. The error bars are the rms error of the 1000 trials which went into finding each point. Fitted with a saturating exponential with equation $P_{det} = A(1 - \exp\left(\frac{-P_i}{B}\right))$ Here A is the parameter p0 and B is the parameter p1

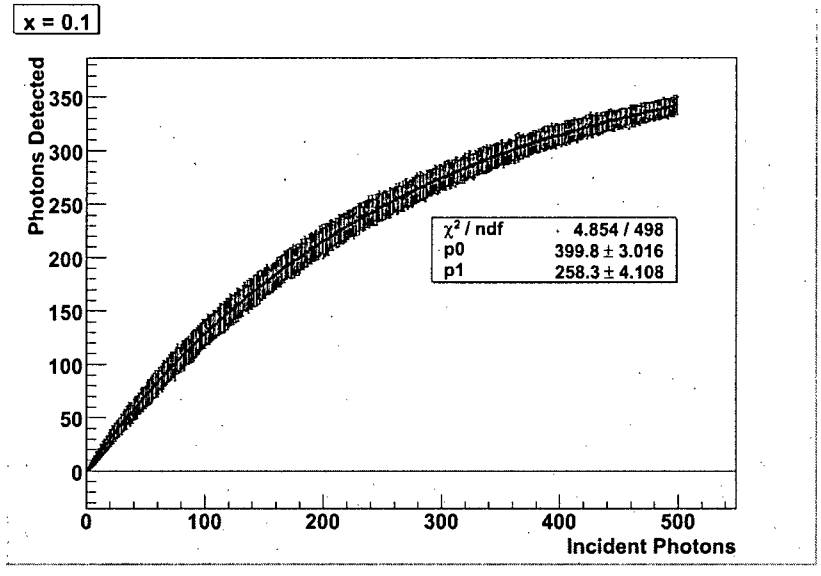

Figure 5.9: Simulated data of fired pixels vs. incident photons for a 400 pixel sensor with crosstalk parameter of 0.1. The error bars are the rms error of the 1000 trials which went into finding each point. Fitted with a saturating exponential with equation $P_{det} = A(1 - \exp\left(\frac{-P_i}{B}\right))$ Here A is the parameter p0 and B is the parameter p1

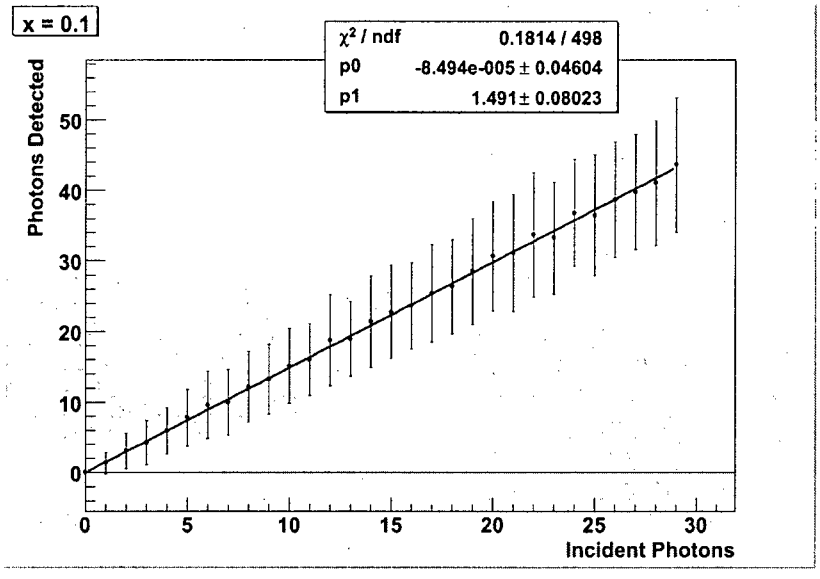

Figure 5.10: Over the first 30-50 pixels in Fig 5.9 is well fitted by a straight line. I defined the slope of this fit as $(firedpixels/incidentphotons)_0$. The error bars are the rms error of the 1000 trials which went into finding each point.

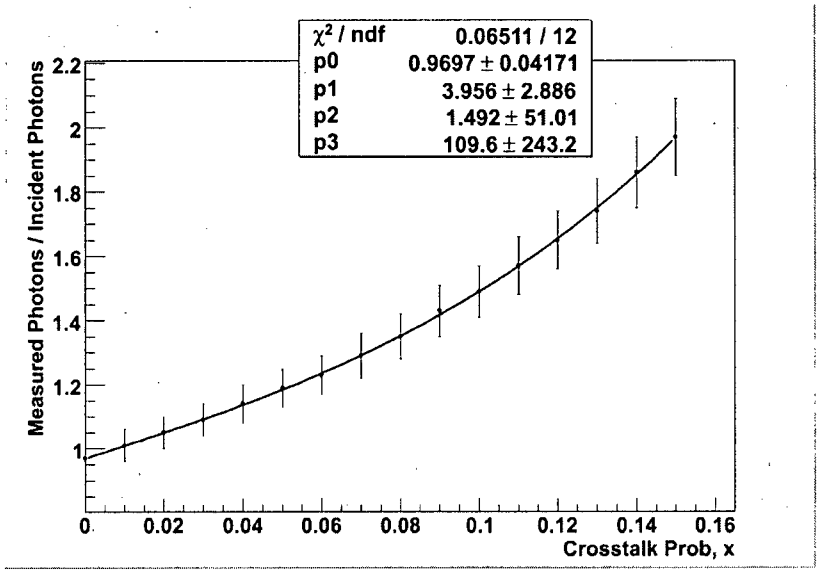

Figure 5.11: $(firedpixels/incidentphotons)_0$ vs. crosstalk probability

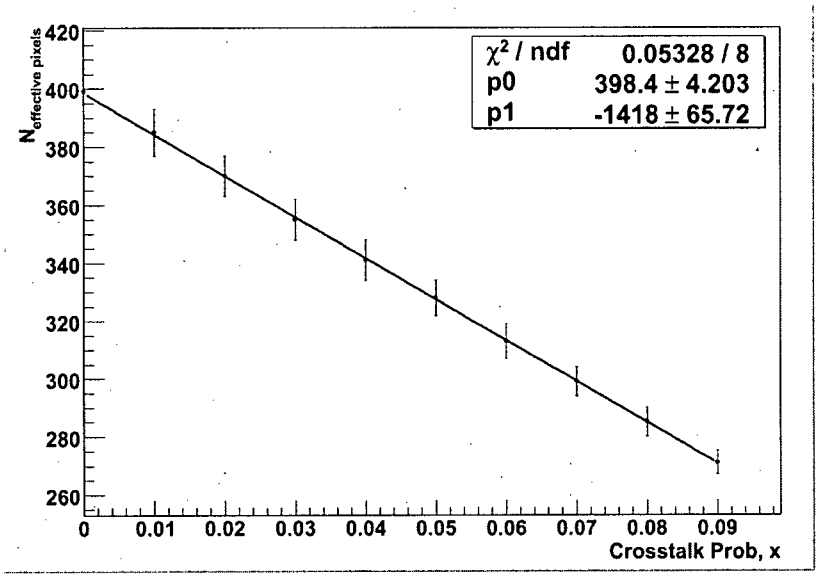

Figure 5.12: Interestingly, plotting the effective pixels fitted parameter vs. cross talk parameter, yields a linear relation. The errors in the points are the errors in parameter B as calculated by the fitting program when fitting the saturating exponential to the photons detected vs. incident photons graph.

5.8 Crosstalk contributions to each peak

The pedestal peak is populated by events where no pixels fire and so crosstalk, which comes from fired pixels, has nothing to do with the population of this peak. The first PE peak comes from when just one pixel is fired in the photosensor. This is not the end of the story however as once this pixel fires none of the neighbouring pixels fire and so from this we can measure the crosstalk rate.

The LEDs should put out the same amount of light each time they are pulsed. Therefore the charge spectrum distribution should be Poisson. We should therefore be able to measure the Poisson rate using the fraction of events in the pedestal and then predict the population of the first photo peak assuming no crosstalk. The difference between the expected number of counts in the first photo peak and the actual number of counts in the first photo peak will be due to crosstalk.

The Poisson Rate λ is found from inverting the equation,

$$\frac{ped}{total} = \exp(-\lambda), \tag{5.2}$$

gives,

$$\lambda = -\ln(\frac{ped}{total}), \tag{5.3}$$

where ped is the population of the pedestal peak and total is the total number of events. From this position rate we can predict the number of events in the first photo peak to be,

$$\frac{one_{expected}}{total} = \lambda \exp(-\lambda), \tag{5.4}$$

where $one_{expected}$ is the population of the 1st photo peak. The difference between the predicted number of 1st photo peak events and the recorded number will be due to crosstalk,

$$one_{actual} = one_{expected}(1-x)^4. \tag{5.5}$$

Here x is the crosstalk parameter, thus $1-x$ is the probability of one neighbouring pixel not firing and $(1-x)^4$ is the probability of the 4 closest neighbors not firing.

We had a problem using this method, however. The population of the pedestal was much higher than the rest of the peaks and so the distributions were obviously not Poisson. We expected this was due to a problem with the LED pulser. We got results as if the LED was pulsed but didnt give out

any light thus giving a larger than expected pedestal population. In other words the problem with the LED made a non-Poisson distribution with an enhanced pedestal.

To get around this problem I had to look at the charge spectrum of the MPPC at the same time as the Russian devices to see if there was any correlation between the two.

To do this I did various cuts. I plotted the charge spectrum for the MPPC with cuts on the number of PEs seen in one of the Russian devices. I plotted 7 MPPC charge spectrums for the numbers of pixels fired in the Russian device from 0 to 6. There was definitely a correlation between pedestal counts in the Russian device and the MPPC which agrees with the LED pulser theory.

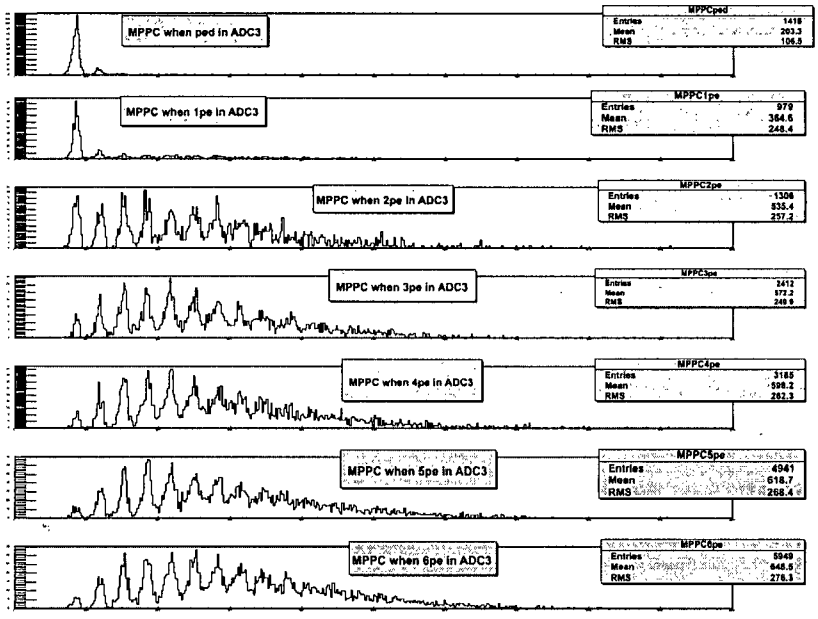

Figure 5.13: Plots of the MPPC charge spectrum for different cuts on the number of PEs produced in the Russian Device (connected to ADC channel 3 or ADC3 for short) for the same event.

I found the crosstalk rate from each charge spectrum using the method described above. I found that for the cuts on the higher number of pixels

fired in the Russian device the crosstalk probability plateaued out. The data takes time to plateau out due to Poisson statistics again. If there is no light produced in one bar, it is not beyond Poisson statistics for there to be 1, 2 or 3 PEs in another bar. The data tends to plateau out around 3 to 4 PEs and therefore is unlikely a fluctuation due to Poisson statistics, and therefore the LED must have fired. In essence, requiring multiple PEs in the Russian SiPM eliminated cases where the LED failed to fire. The plateau value for each different bias run was used to produce a crosstalk vs. photosensor bias voltage plot. This graph was linear so I fitted it with a linear function for later use.

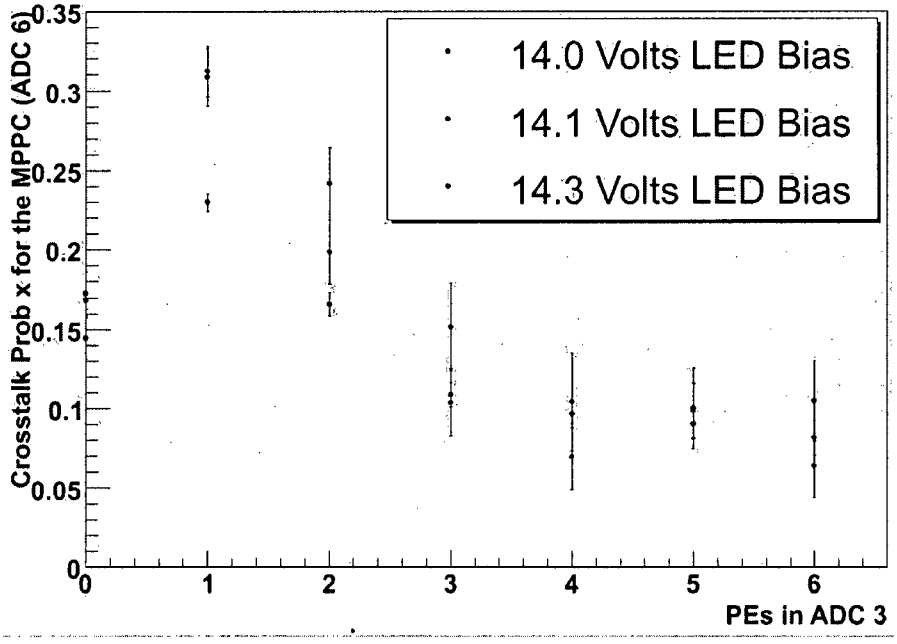

Figure 5.14: Crosstalk parameter for each cut on the number of PEs seen in the Russian device and from 3 different LED bias voltage.

I now had the tools I needed to find the number of incident photons on the photosensor. Knowing the bias voltage I could read off the crosstalk parameter and then use this to find the fraction, fired pixels/incident photons.

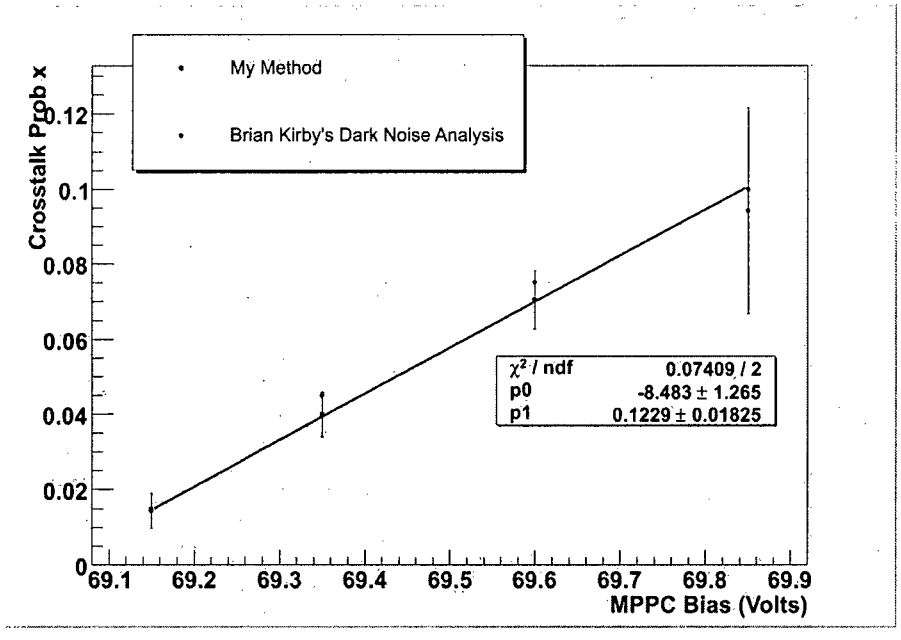

Figure 5.15: Cross talk parameter as a function of bias voltage. Also on the plot is a second series of data taken on the same device using a different technique whereby the dark noise is used to estimate the crosstalk parameter [14].

5.9 Time of flight

To separate the charge collected by the MPPC for the different particles a time-of-flight method was used. A TDC (Time to Digital Converter) measured the time between the particles triggering the first trigger counter and the second. Plotting the charge in one ADC vs. the time of flight (See Figure 5.16) clearly separates the different particles. Therefore to get the charge spectrum for each particle a cut on the time-of-flight can be implemented.

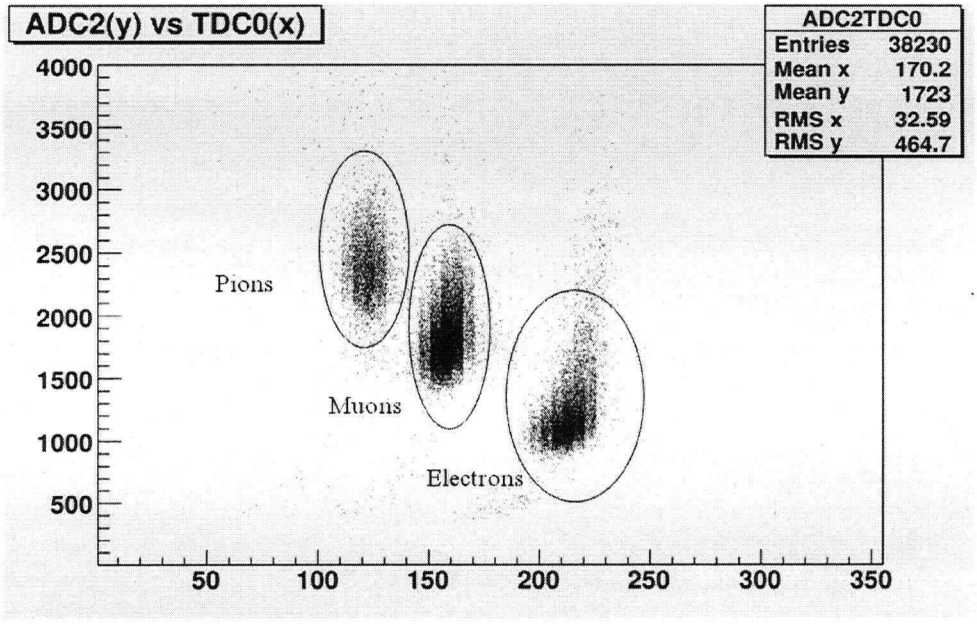

Figure 5.16: Charge deposited in the ADC vs. the time-of-flight. Particles are easily separated. The beam is at a fixed momentum therefore the pions, which are the heaviest of the 3 particles, cross between the two trigger counters in the slowest time and the electrons, which are the lightest of the 3 particles, cross between the trigger counters in the fastest time. The muons come in between.

5.10 MIPS

Over runs 1815, 1816 and 1817 some data was taken using electrons, muons and pions at different voltages. The beam momentum was 120 MeV/c and

the beam hit the bar 195 cm from the readout end.

The pedestal position was found by fitting a Gaussian to it. The peak in the charge spectrum was initially fit with a Gaussian, but after some discussion about the relevance of fitting a Gaussian to the data the mean of the histogram, excluding the pedestal and dark noise peaks, was taken. Figures 5.17, 5.18, 5.19 and 5.20 show these charge spectra.

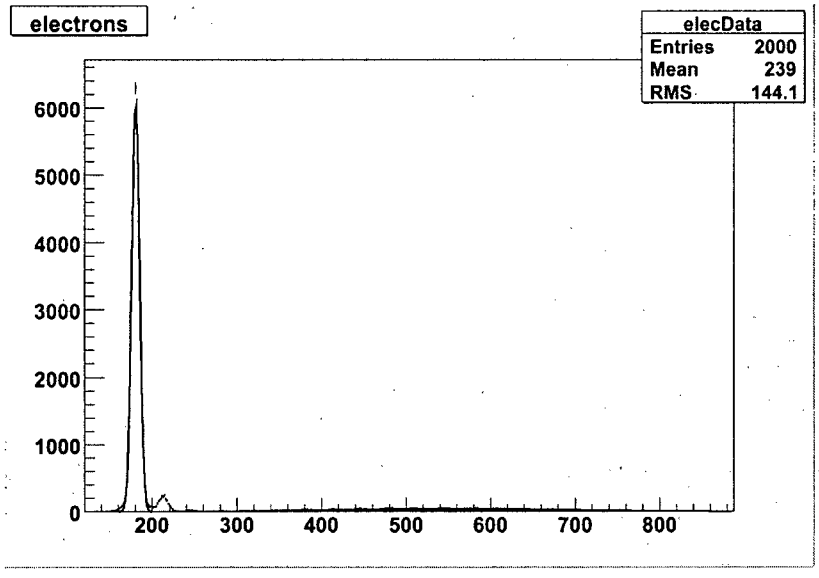

Figure 5.17: Charge Spectrum, just from electrons, for the 1816 Run with a Gaussian fit to the Pedestal. The MPPC bias voltage is 69.3 Volts.

From this data it was simple to work out that the average number of PEs produced when electrons, muon and pions at a momentum of 120 MeV/c pass through the our scintillator bar 195 cm from the readout end is,

$$\text{mean number of PEs} = (\text{mean of the charge spectrum} - \text{pedestal})/\text{gain} \tag{5.6}$$

Figure 5.21 shows the result of these "number of PEs" calculations. The second set of points is the data with a crosstalk correction. For the points at a particular operating voltage the crosstalk probability and then the $(firedpixels/incidentphotons)_0$ is found. The fired pixel number could

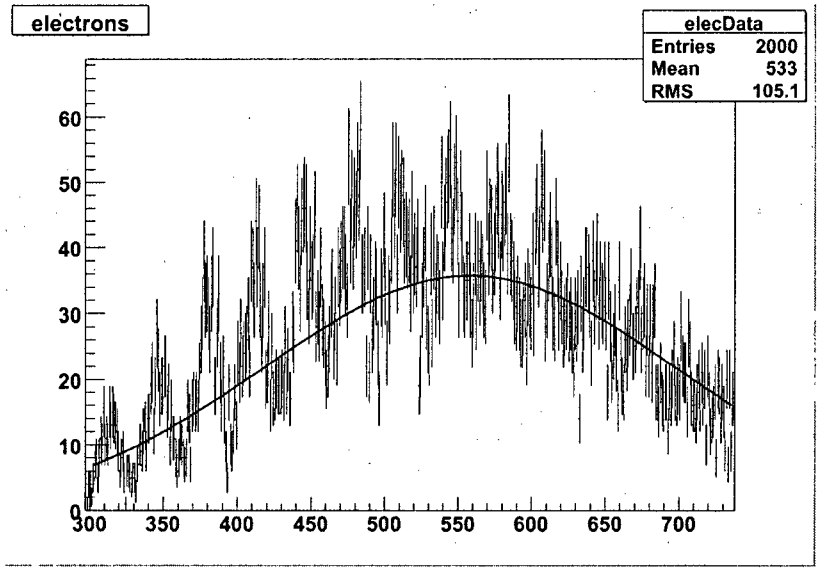

Figure 5.18: Charge Spectrum for the 1816 Run with a time of flight cut to accept only electron hits. The peak in the charge spectrum is zoomed in on and is fit with a Gaussian function. The MPPC bias voltage is 69.3 Volts.

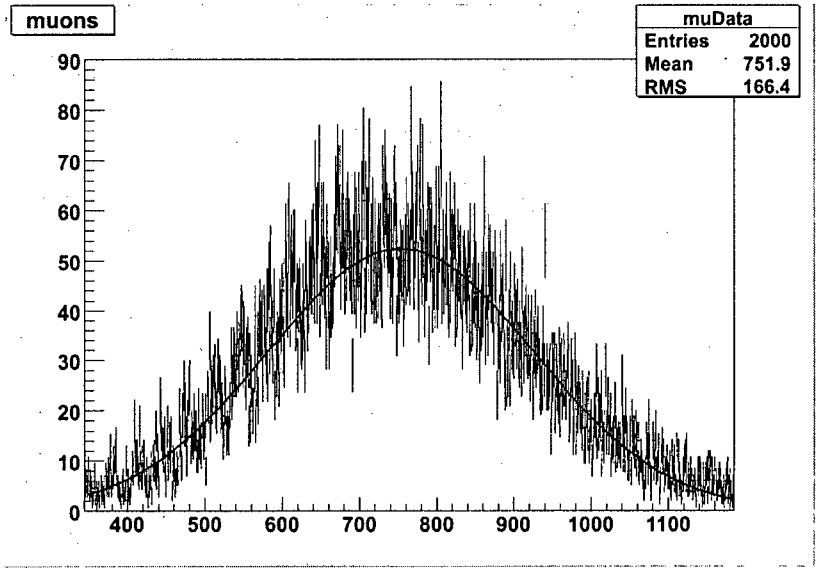

Figure 5.19: Charge Spectrum for the 1816 Run with a time of flight cut to accept only muon hits. The peak in the charge spectrum is zoomed in on and is fit with a Gaussian function. The MPPC bias voltage is 69.3 Volts.

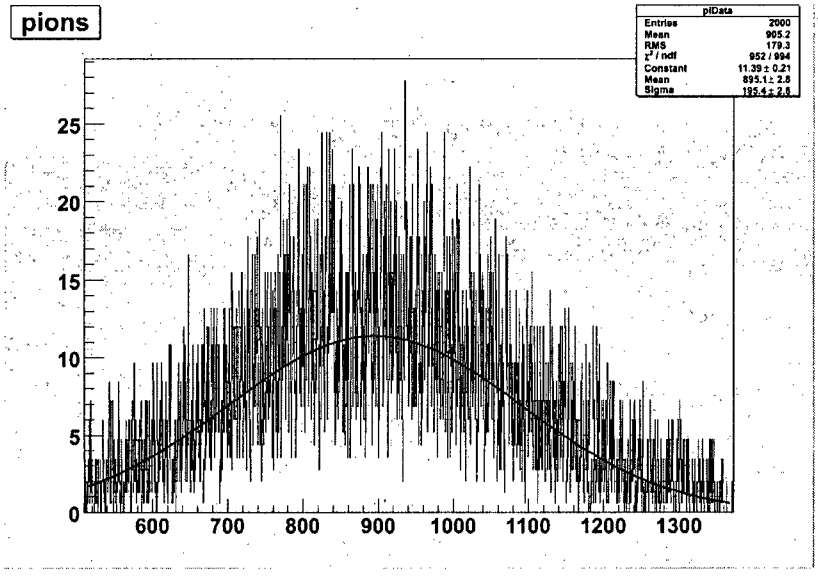

Figure 5.20: Charge Spectrum for the 1816 Run with a time of flight cut to accept only pions hits. The peak in the charge spectrum is zoomed in on and is fit with a Gaussian function. The MPPC bias voltage is 69.3 Volts.

then be divided by this ratio to get the incident photons for the data set. We have a requirement that we want the MPPCs to see greater than 15 PEs from a MIP (the electron is a MIP at 120 MeV/c) passing through the far end of the bar. We will mirror the far end of the bar which will increase the light yield by 70%. After mirroring out light yield from electrons will be greater than 15 PEs even at a voltage as low as 69.3 Volts.

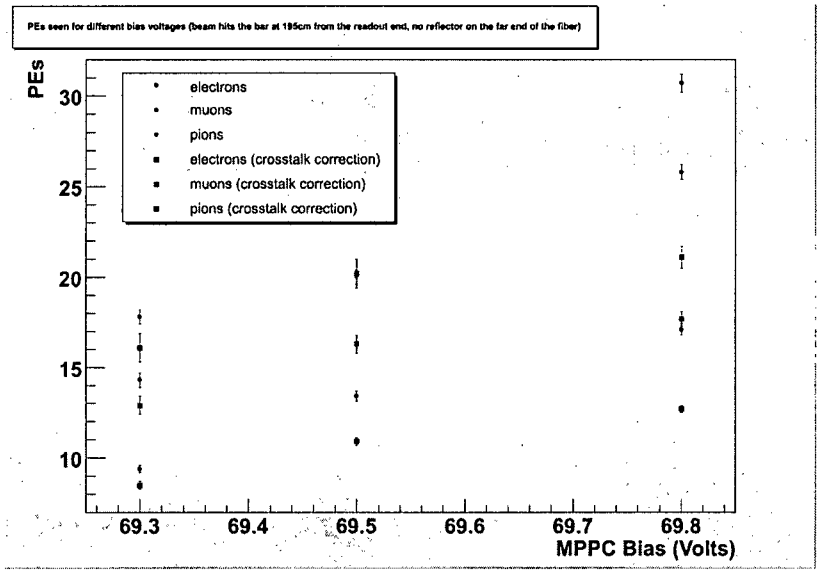

Figure 5.21: Number of photoelectrons produced, for different particles, as a function of bias voltage with and without crosstalk and saturation correction. Errors are the standard error about the mean of the previous histograms.

5.11 protons

After we took the good data using the electrons, muons and pions some hardware died and we were only left with one channel. We decided to take data with the Russian photosensor at a 47.5 V bias voltage. We did runs reading out each bar/fiber in turn where the beam was incident on the bars 50, 100, 150 and 195 cm from the readout end. This data is show on Figure 5.22. I took the mean of this data and plotted this again (See Figure 5.23).

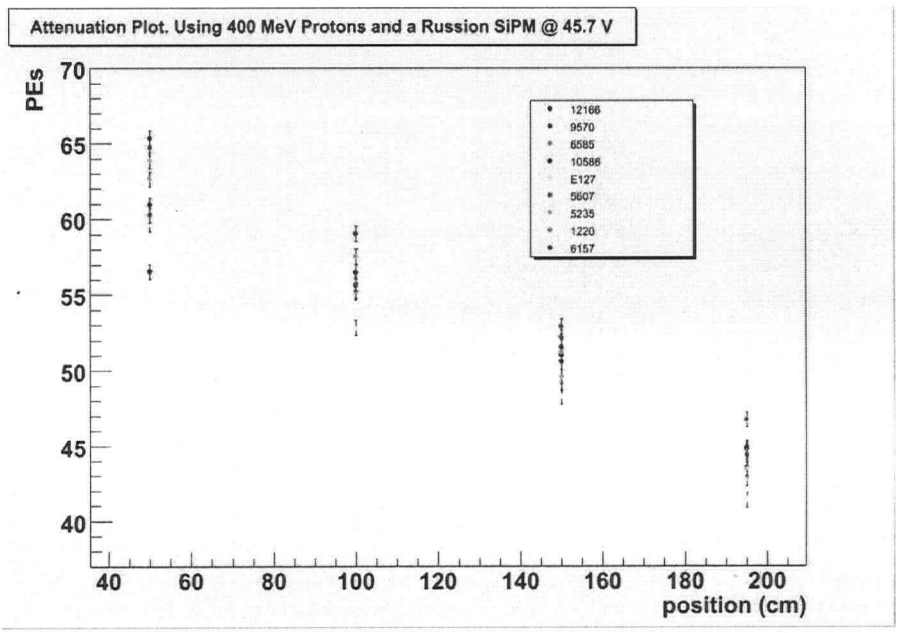

Figure 5.22: Light Yield from Protons as a function of position for the 9 different bars

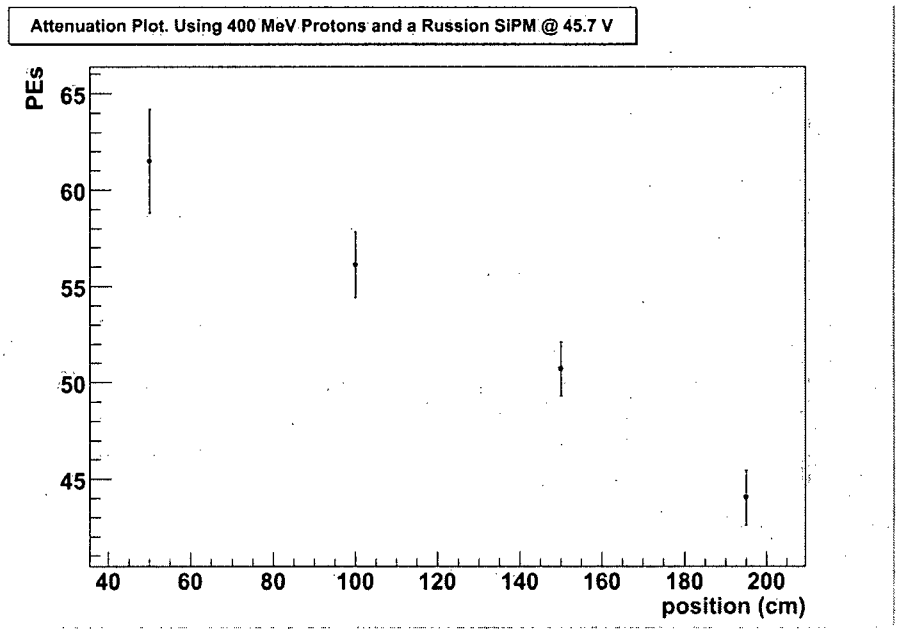

Figure 5.23: Average Light Yield from Protons as a function of position. The errors are taken to be the rms of the points in Figure 5.22.

5.12 Predicting dE/dx

From the M11 beam test we have, for fixed photosensor bias voltages, numbers of PEs produced from each particle having a certain energy.

Now we need to check that the ratios of PEs produced from each particle agrees with dE/dx predictions.

dE/dx values give the rate of energy loss of particles as they pass through a certain distance through the target medium.

The Bethe-Bloch equation (found in the particle data book [10] gives the dE/dx values for particles which are heavy relative to the electron, thus it works very well for muons, pions and protons.

$$-\frac{dE}{dx} = Kz^2\frac{Z}{A}\frac{1}{\beta^2}\left(\frac{1}{2}\ln\frac{2m_ec^2\beta^2\gamma^2T_{max}}{I^2} - \beta^2 - \frac{\delta(\beta\gamma)}{2}\right) \tag{5.7}$$

where Z is the atomic number of the absorber, z is the charge of the incident particle, A is the atomic mass of the absorber ($gmol^{-1}$), m_e is the mass of the electron, I is the mean excitation parameter, β and γ are the usual relativistic ratios and T_{max} is given by,

$$T_{max} = \frac{2m_ec^2\beta^2\gamma^2}{1 + 2\gamma m_e/M + (m_e/M)^2}. \tag{5.8}$$

In the particle data book the min dE/dx for muons is quoted to be 1.936 for polystyrene scintillator. I tuned the parameter I (which has no quoted value) for muons until the minimum of the dE/dx curve was equal to 1.936. Having found this tuned value I check my function at various other points and compared it to the dE/dx plots in the particle data book. The agreement between the two was great.

Figure 5.24 shows a plot of my tuned dE/dx functions for different particles. Electrons are assumed to be minimum ionizing so are essentially always at 1.936 over this range.

Table 5.3 shows dE/dx values for the particles we used at the momentum we used them.

I took the data using the Russian device and electrons, pions, muons and protons as incident particles. Unfortunately there was not data taken with the MPPCs and protons as the incident particles. The mean number of PEs produced from each particle is recorded in the table below and put adjacent to the dE/dx predictions.

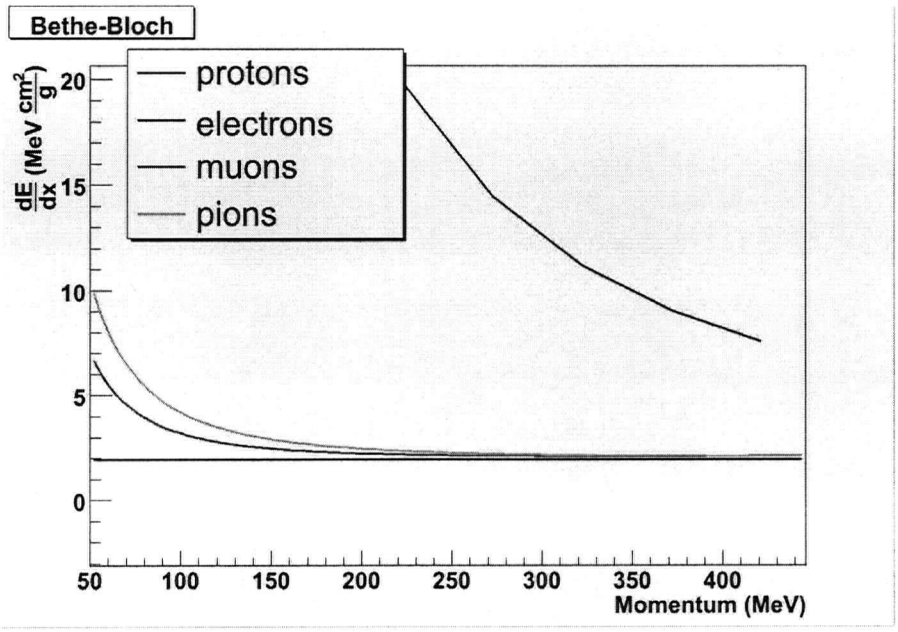

Figure 5.24: dE/dx curves for protons, electrons, muons and pions

Table 5.2: dE/dx predictions

Particle	dE/dx	Ratio to electron at 120 MeV/c
electron @ 120 MeV/c	1.936	1
muon @ 120 MeV/c	2.794	1.443
pion @ 120 MeV/c	3.488	1.801
proton @ 400 MeV/c	8.142	4.205

Table 5.3: Table comparing the actual data with dE/dx predictions. Russian sensor was used and had a bias voltage of 45.7 Volts. The beam hit the far end of the bar 195 cm from the readout end. The Errors in the mean number of PEs are the approximate standard errors ($rms/\sqrt{N}$) of the data about the mean. The errors in the ratio to electrons have been calculated by propagating the error in the mean number of PEs.

Particle	mean number of PEs	Ratio to electron	dE/dx ratio predictions
electron @ 120 MeV/c	11.0 ± 0.1	1	1
muon @ 120 MeV/c	15.8 ± 0.1	1.43 ± 0.02	1.43
pion @ 120 MeV/c	19.7 ± 0.1	1.79 ± 0.03	1.801
proton @ 400 MeV/c	45.7 ± 0.1	4.15 ± 0.05	4.205

Chapter 6

Light Output from Fiber

6.1 Wavelength Shifting Fibers

When a charged particle travels through one of our scintillator bars it slows down, depositing energy which in turn will be converted into light. We catch that light using a WLS (Wavelength Shifting) fiber, which runs down the center of that bar, and then detect the light as it comes out of the end of the fiber.

The WLS Fiber works on the principle that it absorbs a certain range of wavelengths (we choose this to cover the wavelength of the scintillated light) and emits over a different range of wavelengths. Light from our scintillator bars will pass across the WLS fiber. This light will be absorbed at random radial positions in the fiber. The WLS fiber will then emit the light in all directions at a lower wavelength. Some of this light will travel at an angle such that it will not escape the fiber and will makes it way in both directions total internal reflecting until it gets to the end of the fiber. Figure 6.1 shows the absorption and emission spectrum for the WLS fiber we will be using in the FGD. The fiber strongly absorbs blue light and the re-emits green light.

The fiber is also multi-clad rather than single clad. This improves the light yield of the fiber as the fiber has a much higher trapping efficiency than a single clad fiber when it re-emits the light. With a second cladding the acceptance angle for a photon traveling in the fiber is anything less than 26.7 degrees (See Figure 6.3), for a single laded fiber this angle is just 20.4 degrees (See Figure 6.2). The solid angle for a right circular cone is,

$$4\pi \sin^2 \theta/2, \tag{6.1}$$

and so the ratio of light trapped in the multi clad fiber to the single clad fiber is,

$$\frac{4\pi \sin^2 26.7°/2}{4\pi \sin^2 20.4°/2} = 1.303, \tag{6.2}$$

so the light yield turns out to be 30 % higher for the multi-clad fiber over the single clad fiber.

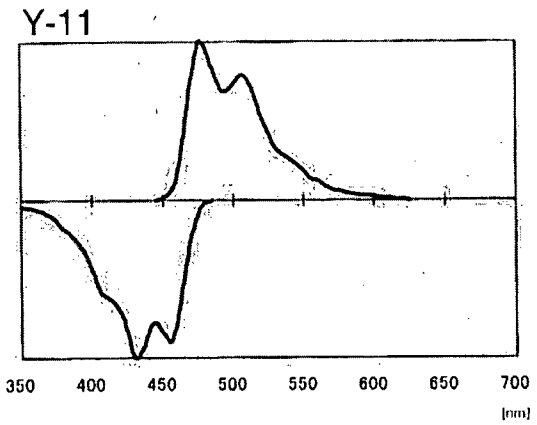

Figure 6.1: Emission (above) and Absorption (below) Spectra for our WLS Fiber [15].

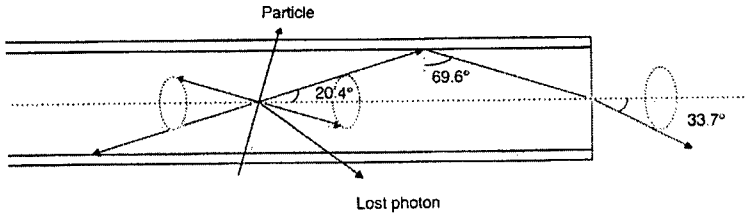

Figure 6.2: Figure showing a cross section of a single fiber. Photons emitted within an angle of 20.4 degrees with respect to the fiber axis are trapped and will make it to the end of the fiber.

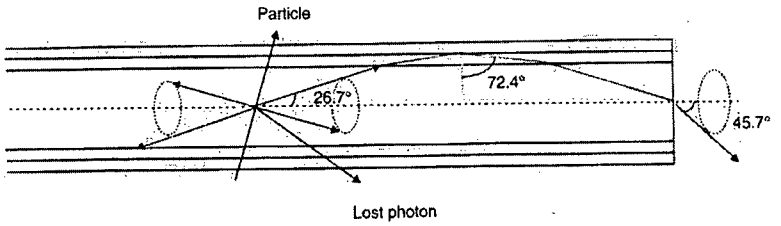

Figure 6.3: Figure showing a cross section of a single fiber. Photons emitted within an angle of 26.7 degrees with respect to the fiber axis are trapped and will make it to the end of the fiber.

Table 6.1 gives material, refractive index and density information on the core and cladding components of the fiber.

Table 6.1: Fiber Material Properties [15]

	Material	n	$\rho(grams/cm^3)$
core	Polystyrene	1.59	1.05
inner cladding	Polymethylmethacryolate	1.49	1.19
outer cladding	Fluorinated Polymer	1.42	1.43

When the light comes out of the end of the fiber it isn't uniformly distributed however. As we look at the end of the end of the fiber we can define an angle ϕ that we view the end of the fiber at as the angle between our line of sight and the normal vector to the end of the fiber. See Figure 6.4

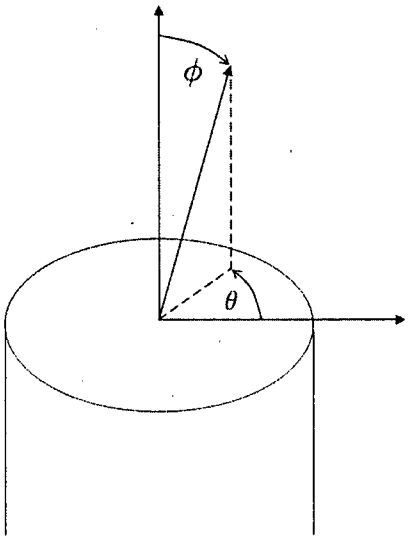

Figure 6.4: Coordinate system with respect to the fiber

Up to an angle of around 45 degrees the end of the fiber has a roughly uniform brightness all over. Over 45 degrees a vertical dark band appears whose width increases as the angle you view the end of the fiber at increases. See figure 6.5.

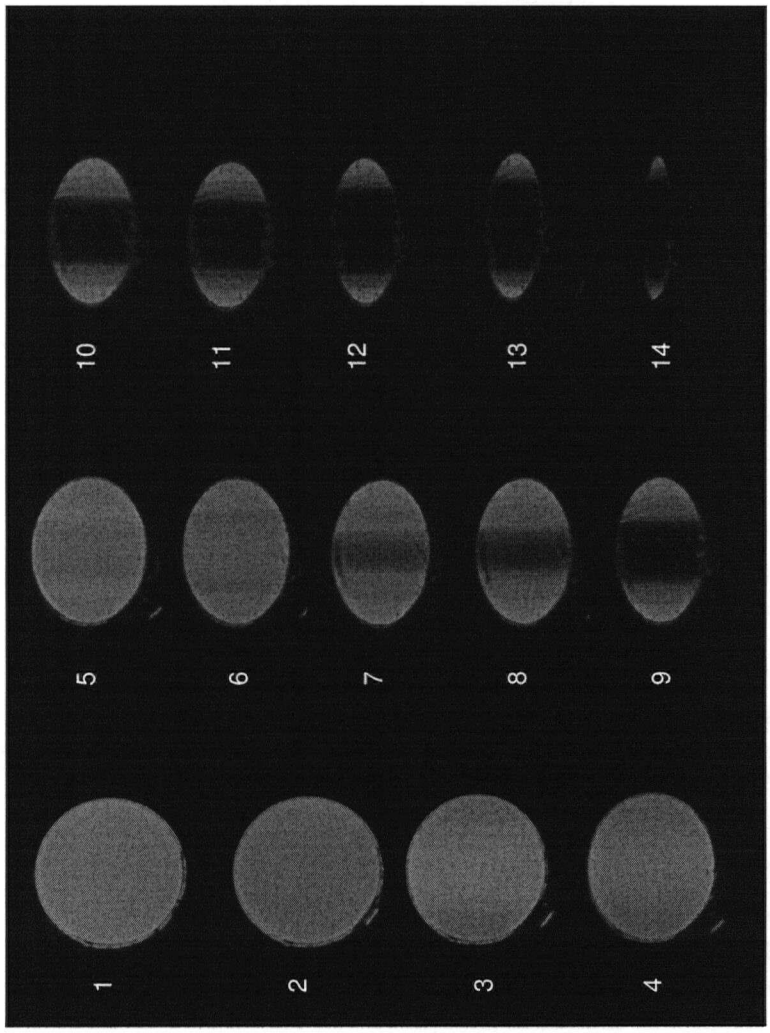

Figure 6.5: photos of the end of the WLS fiber (Illuminated using a UV lamp 1m from the end, photos taken using a LEICA DFC320 CCD camera (3.3Mpixels, 7.2mm x 5.35 mm sensitive area) mounted on a LEICA microscope) at different angles with respect to the fiber axis. 1 = 0°,2 = 10°,3 = 20°,4 = 30°,5 = 40°,6 = 45°,7 = 50°,8 = 52.5°,9 = 55°,10 = 57.5°,11 = 60°,12 = 65°,13 = 70°,14 = 80°

6.2 Light Distribution Physics

The physics behind this band forming is related to skew rays. The light from the scintillator bar can be absorbed at any radial point of the fiber. Some of the re-emitted photons start with such an angle that they will just spiral around the edge of the fiber and will never cross the center of the fiber. These rays are known as skew rays.

Figure 6.6 shows a sketch of the end of the fiber with the vertical lines representing the edges of the dark band. The skew rays to first order travel around the edge of the fiber along the dashed line path.

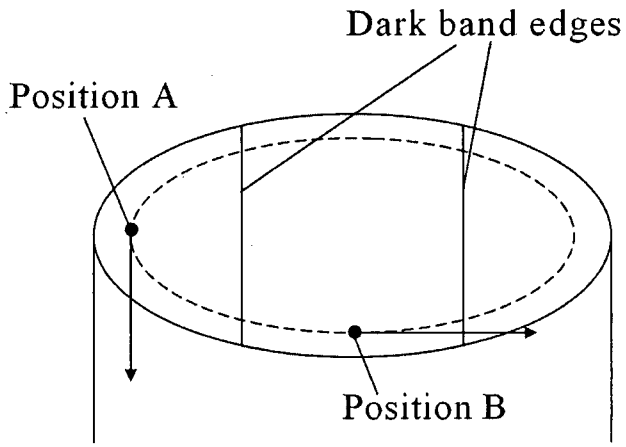

Figure 6.6: Figure showing two possible exit locations of a skew ray from the end of the fiber with respect to an observer at some angle θ and ϕ

Consider two points, A and B, where the skew ray might exit the end of the fiber. At point A the skew ray will be traveling towards us and when it leaves the fiber we will see it. At point B the skew ray will exit the fiber and we will not see it as it will be traveling to the right. Note that if you looked at this fiber from the right you would see the photon from point B and not A. Therefore no matter how you look at the fiber (at a particular ϕ angle) the dark band will always appear vertical. We also see light on the other side of the fiber from A. This will be from skew rays which travel in the opposite direction as it propagates down the fiber.

6.3 Fiber Light Output Distribution

I wanted to measure the light output distribution from the fiber for later use in a Monte Carlo Program. I was interested in finding two things: the total intensity as a function of ϕ and the intensity profile as a function of ϕ

For light to come out of the end of the fiber I needed to illuminate the WLS fiber using a UV lamp (the wavelength distribution of the UV lamp was thought to represent the wavelength distribution of the scintillated light in the polystyrene bars).

The lamp was placed adjacent to the fiber 1m from the end of the fiber. The end of the fiber was then placed under a microscope so a photo could be taken of if it. The image was taken with a LEICA DFC320 CCD camera (3.3Mpixels, 7.2mm x 5.35 mm sensitive area) mounted on a LEICA microscope. Photos of the fiber were taken at different angles between 0 and 90 degrees with respect to the fiber axis (See Figure 6.5). I wanted to take a picture so that none of the pixels were completely saturated but also wanted to maximize the exposure to get a better signal to noise ratio. I did this in a trial and error fashion playing with the exposure length setting on the camera.

Once I had photos of the fiber at each angle I could analyze them.

The tool I used for the analysis was called ImageJ [12]. It is a small stand alone java program which will give you the information about each pixel. It has a histogram feature whereby one can highlight a profile across the fiber and then have the program give you the brightness distribution across that profile, the data is then output in a text file for analysis. Figure 6.7 is a plot of these brightness profiles.

In addition to the intensity profile distributions I also found total intensity values as a function of ϕ. This was done in ImageJ simply by highlighting the entire end of the fiber in the photograph and then adding up the intensity of all the pixels. Figure 6.8 is a plot of these total intensities. This plot was best fitted using two functions for later use in a Monte Carlo.

$$T(\phi) = \begin{cases} 0.99611 + 0.00070\phi - 0.00015\phi^2 & \text{if } 0 \leq \phi \leq 55; \\ 0.49717\exp(-0.15235(-52.5 + \phi)) & \text{if } 55 < \phi \leq 90. \end{cases} \tag{6.3}$$

where $T(\phi)$ is the Total Intensity as a function of ϕ.

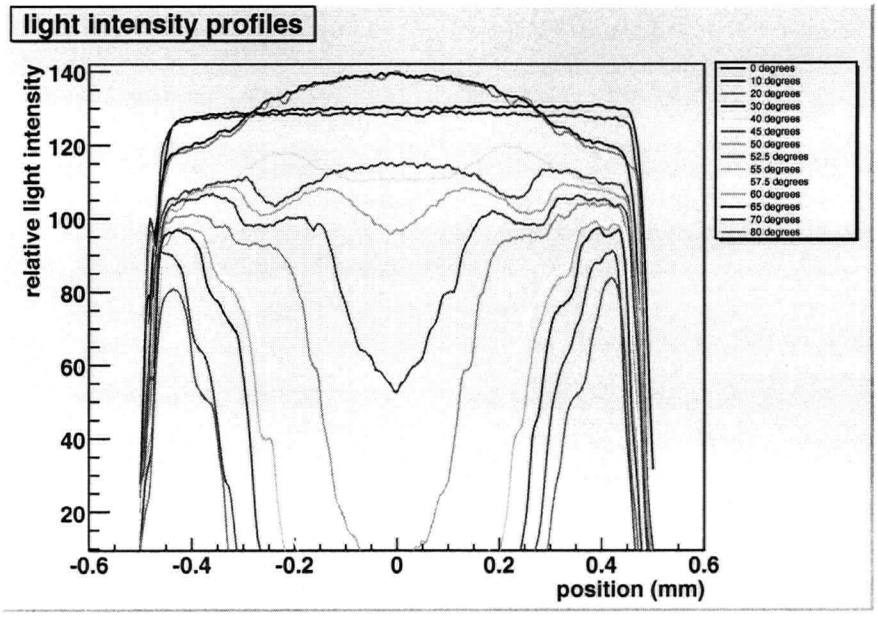

Figure 6.7: Light Intensity Profiles

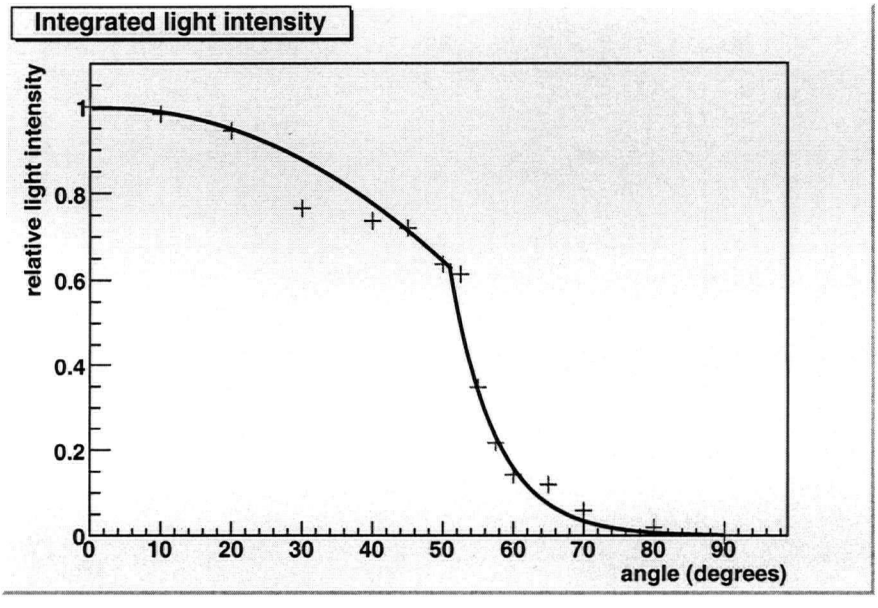

Figure 6.8: Total Light Intensities

6.4 Light Loss

It is likely that the active area of our photosensor is not butted up directly against the end of the fiber. The photosensor will have a thin epoxy coating over the active area to protect it from damage. Now I have total light intensity and light intensity profiles for different ϕ I could simulate photons coming from the end of the fiber with this distribution and then see how many of the photons make it to the photosensor.

6.5 Simulation

6.5.1 Generating photons

I wanted to produce photons that originated on the surface of the fiber and come away from the fiber with a distribution very close to what I observed and measured using the microscope. The choice of coordinate system is not obvious, with the fiber having a circular end and the photosensor being square. I chose eventually to use a couple of coordinate systems, first generating photons in spherical coordinates and then moving to Cartesian coordinates for the ray tracing.

Each photon needs to be generated to have a starting position vector (x, y, z) and a starting velocity vector ($\dot{x}$,$\dot{y}$,$\dot{z}$). Finding the velocity is more straight forward than the starting position so I calculate this first. The intensity profile plots I produced from the microscope data are for different ϕ angles (where $\phi = 0$ is perpendicular to the surface of the end of the fiber and $\phi = 90$ is parallel to the surface of the end of the fiber) and so I want to generate a starting ϕ angle for the photon based on this data.

First of all the angle θ is chosen randomly to be between 0 and 2π, i.e. there is no preferred θ direction. This was seen experimentally that if you look at the fiber and rotate the end, looking at it at constant ϕ, the light distribution stays the same.

The ϕ direction takes a more involved calculation. Firstly, larger ϕ angles are favoured by solid angle, using a sine curve as the basis of an acceptance-rejection technique. If you have a unit length arrow coming from the fiber at a particular ϕ angle, projecting it on to the theta plane and rotating it by 2π in the θ coordinate to make a circle the circumference of that circle is proportional to $\sin\phi$. Thats why there is a sine weighting as there is more solid angle for the photon to move into at higher ϕ values.

In my code the random selection of a ϕ angle is also weighted by the total light intensities by implementing another acceptance-rejection technique

(See Figure 6.8).

Now that we have a θ and ϕ angle for the photon we can calculate the velocity vector for the photon. This is done by giving the velocity vector unit length in spherical coordinates and then transforming to Cartesian coordinates.

We now need a starting position for the photon on the surface of the end of the fiber. I can define x-y coordinates for this with the $\theta = 0$ direction being the x axis and the y axis perpendicular to the x. The intercept of these axes is in the center of the end of the fiber. There are intensity profiles for 14 different ϕ angles. The closest of these angles to the angle ϕ of our photon is chosen and that particular intensity profile is used to generate a starting position for the photon. An x starting position is chosen for the photon using the intensity profile for an Acceptance-Rejection technique. The y position is then generated between $+D/2$ and $-D/2$, the full width of the fiber at its widest point is D, and then if it falls within the real bounds of the fiber at that x it is accepted. If this y value is rejected then x value is also rejected and we start again and generate a new x.

Each photon will have their own unique x-y coordinate system (given by θ). I chose to define a fixed x-y coordinate system where the x axis is in the direction of the $\theta = 0$ direction. I could find a starting position for the photons in terms of this coordinate system simply by doing a rotation by θ degrees.

6.5.2 Do the photons hit the photosensor?

Now we have a starting position vector and a unit velocity vector the rest of the problem is ray tracing.

The photosensor is a fixed distance from the end of the fiber. The surface of the photosensor defines the photosensor plane so having the initial position and unit direction vector of the photon, the intercept of the photon with the photosensor plane can be found. Next you just have to check that the photon hit the photosensor itself so you look to see which photons hit the photosensor plane within the bounds of the photosensor. For each one that does you add it to the total that did hit the photosensor.

6.5.3 Epoxy Coating

The photosensors come with an epoxy coating to protect the surface of the chip. My code has the option of having a refractive medium between the fiber and the photosensor so its effects can be noted. For simplicity the

refractive medium has two surfaces which are parallel to the planes defined by the end of the fiber and of the photosensor. In reality the outer surface of the epoxy coating is unlikely to be flat. Prototypes of the Russian Device tend to be convex and the MPPC tend to be concave. The code also assumes that the end of the fiber will be butted directly up against the epoxy coating. This might not be entirely correct as out fiber-photosensor coupler may not perfectly butt the fiber up to the photosensor.

The initial starting position of the photon on the fiber is then equal to the initial starting position of the photon in the refractive medium. The unit velocity vector of the photon is adjusted for its path through the refractive medium using a refractive index of 1.5 (typical refractive index of epoxy). This is a simple process of slowing the photon down in the x and y direction by the fraction $\frac{n_{air}}{n_{plastic}}$ and adjusting the length in the remaining z direction so the direction vector is still of unit length.

The x-y position of the photon where it exits the refractive medium, which has a set thickness, can be found using the initial position vector and the unit velocity vector of the photon inside the medium. From then on the position where the photon hits the photosensor plane can be found from using the refractive medium exit position and the initial velocity vector before the photon entered the refractive medium.

6.5.4 A sideways offset between the fiber and the photosensor

Having a sideways offset between the fiber and the photosensor is easy to implement. Once you have the final positions of the photons on the plane of the photosensor you can check to see that the photon is within the bounds of the photosensor given it has an offset.

6.6 Results

6.6.1 Fiber-Photosensor Separation

Figure ?? contains a lot of information. For a few photosensor sizes it gives, with and without epoxy between the fiber and the photosensor, the fraction of light that gets to the sensor for different fiber-photosensor separations.

Some results of note

- For a 1 mm square sensor butted up directly against the fiber 100% of the light from the fiber should reach the sensor. Increasing the

separation to 0.4 mm (The minimum specification from Hamamatsu) the amount of light detected goes down to just 35 %

- Assuming the 0.4 mm minimum gap is filled with epoxy (the protective coating for the photosensor) the amount of light that hits the sensor will just go down to 77 %. This confirms that the epoxy, if flat and parallel to the surface of the fiber and sensor on both sides, will focus the light onto the photosensor.

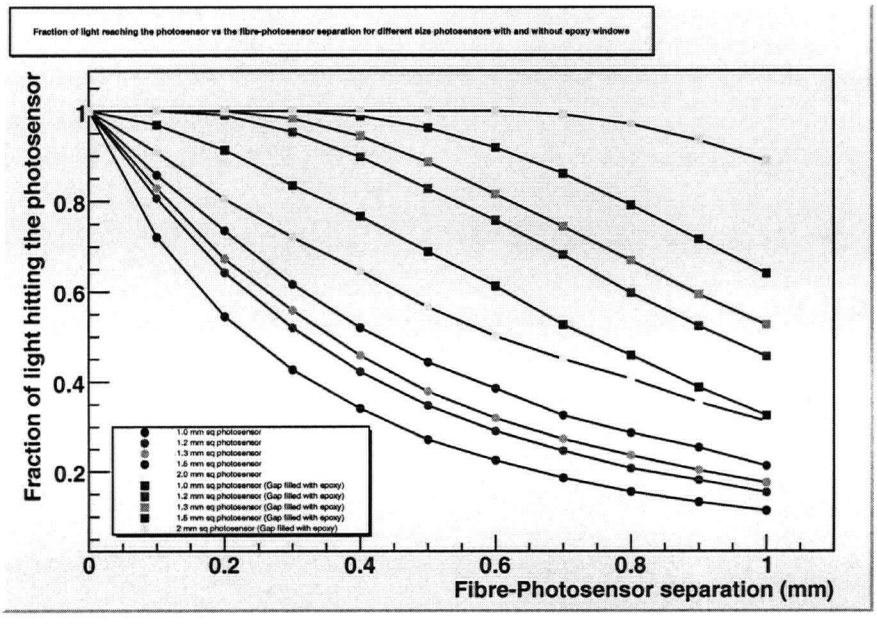

Figure 6.9: Fraction of light that hits the photosensor, for different sized sensors with and without epoxy, as a function of fiber-photosensor separation

At this stage there are two possible sizes of photosensor we could order from Hamamatsu, a 1 mm square photosensor or a 1.3 mm square photosensor. We want an idea of how much more light the 1.3 mm sq photosensor might see so I took the ratio of these curves with and without the epoxy coating (Figure 6.10). With epoxy and the fiber photosensor separation at 0.4 mm it looks like the 1.3 mm sq photosensor will see 25% more light than the 1 mm sq photosensor. We have to balance this improvement against other factors like the noise rate increasing to see which photosensor we want to purchase. On August 1st in a FGD meeting, Kyoto group presented their

measurements on 1 mm sq and 1.3 mm sq MPPCs [16]. Both photosensors are set back in their packaging by 0.47 mm. There is an expoxy window filling this 0.47 mm gap. They measured a light yield ratio between the two of 1.26. This is in good agreement with my simulated result.

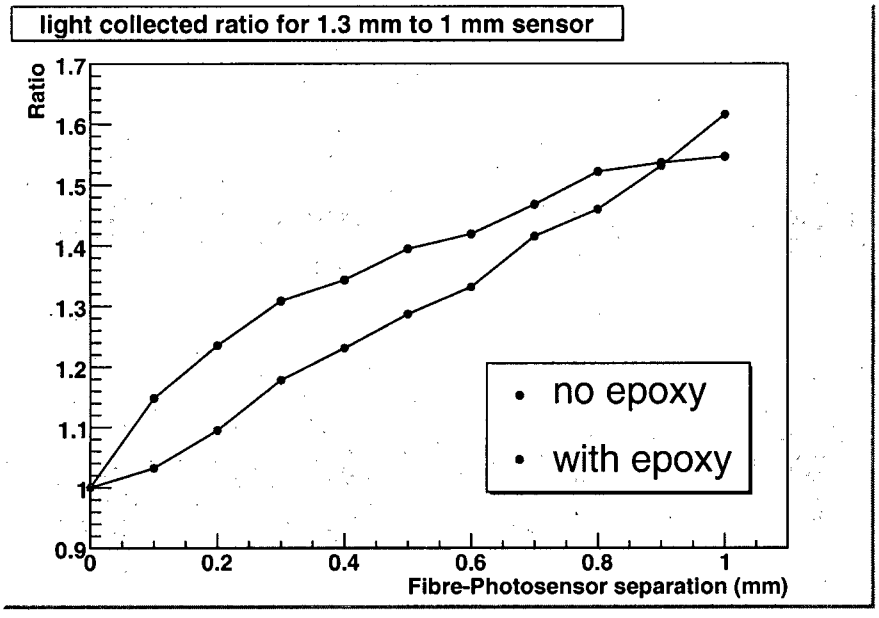

Figure 6.10: Ratio of the Fraction of light hitting the 1.3 mm sq photosensor vs. the 1 mm sq photosensor, with and without epoxy, as a function of distance

6.6.2 Fiber-Photosensor sideways offset

There are two possible problems which could cause a sideways offset between the photosensor and the fiber.

- The photosensor itself comes glued to a plastic packaging with the epoxy coating put over the top. If it is glued off center the fiber and photosensor will not line up properly and light may be lost.
- The fiber-photosensor coupler may also not be perfect causing misalignment issues.

Figure 6.11 shows the fraction of photons which get to the phtotosensor, for two different photosensor sizes, as a function of the sideways offset

between the fiber and the photosensor without an epoxy coating.

Perhaps more relavent, Figure 6.12 shows the same thing but with epoxy filling the distance between the photosensor and the fiber. For an offset less than 0.2 - 0.3 mm there isn't a significant amount of light loss, any more than this the light loss becomes much more significant.

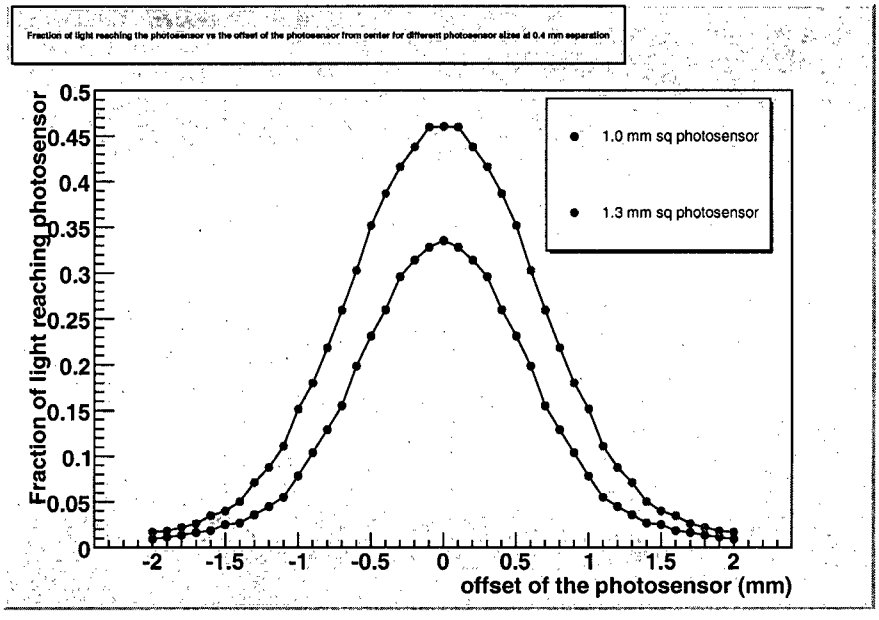

Figure 6.11: Fraction of light reaching the photosensor, as a function of a sideways offset between the end of the fiber and the photosensor, for a 0.4 mm fiber photosensor separation and no epoxy coating in between

6.6.3 photon density on photosensor plane

I wanted to get an idea of the density distribution of the photons across the photosensor. To do this I took the following steps

1. From the final x and y coordinates of the photons find the distance, r, from the center of the photosensor $r_{final} = \sqrt{x_{final}^2 + y_{final}^2}$
2. Calculate a cumulative distribution, $f(r)$ = number of photons with $r < r_{final}$

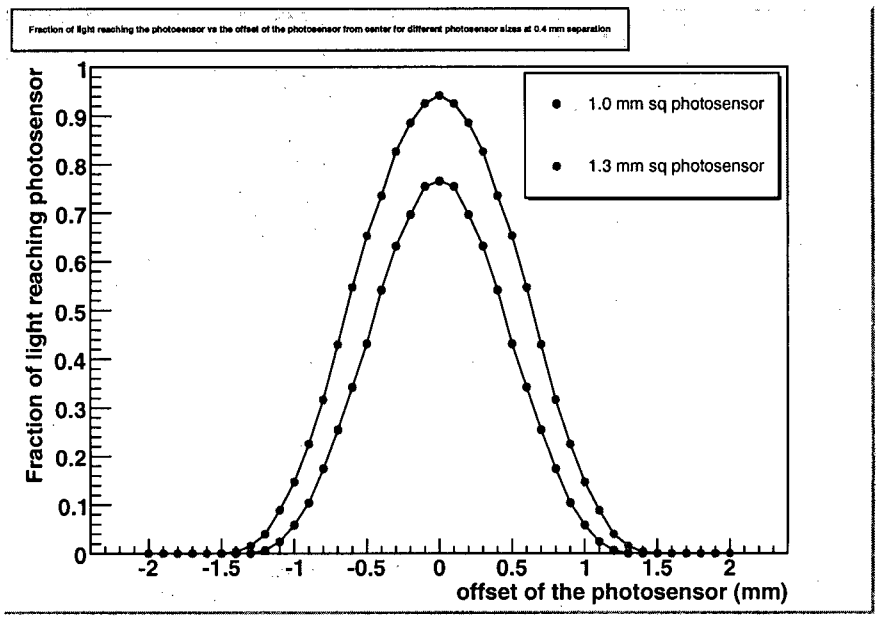

Figure 6.12: Fraction of light reaching the photosensor, as a function of a sideways offset between the end of the fiber and the photosensor, for a 0.4 mm fiber photosensor separation and an epoxy coating in between